

Article

The Petrology and Geochemistry of REE-Enriched, Alkaline Volcanic Rocks of Ambitle Island, Feni Island Group, Papua New Guinea

Olive L. Ponyalou ^{1,*}, Michael G. Petterson ^{2,*}  and Joseph O. Espi ³

¹ Geological Survey Division, Mineral Resources Authority, Port Moresby 121, Papua New Guinea

² School of Science, Faculty of Health and Environmental Sciences, Auckland University of Technology, Auckland 1142, New Zealand

³ Earth Sciences Division, University of Papua New Guinea, Port Moresby 134, Papua New Guinea; joseph.espi@upng.ac.pg

* Correspondence: oponyalou@mra.gov.pg (O.L.P.); michael.petterson@aut.ac.nz (M.G.P.)

Abstract: Ambitle in the Feni Island Group is located within the NW trending Tabar–Lihir–Tanga–Feni (TLTF) volcanic island chain, Melanesian Arc, northeastern Papua New Guinea. The TLTF chain is renowned for its alkaline magmatism, geothermal activity, copper–gold mineralization, and world-class gold mining. Although its geochemical patterns indicate island arc signatures (i.e., high LILE and depleted HFSE), TLTF volcanism is not directly related to the older Melanesian Arc subduction system. However, it may have been influenced by source mantle metasomatism linked to the older subduction. The purpose of this study is to (1) present and interpret the petrographic, mineralogical, and geochemical data from Feni within the context of the tectonic evolution of the TLTF and (2) propose a geodynamic, petrogenetic model for the Feni volcanic rocks. The key methodologies used in this study are field mapping and sampling, petrographic analysis using the optical microscope, whole-rock geochemical analysis via XRF and ICP MS, and mineralogical analysis using an electron microprobe. The main rock types sampled in this study include feldspathoid-bearing basalt, trachybasalt, phonotephrite, trachyandesite, and trachydacite. Minerals identified include forsteritic olivine, diopside, augite, labradorite, andesine, anorthitic plagioclase, nepheline, and leucite in the primitive mafic suites, whereas the more evolved intermediate and felsic hypabyssal suites contain amphibole, albite, orthoclase, biotite, and either rare quartz or feldspathoids. Amphibole composition is primarily magnesiohastingsite with minor pargasite formed under polybaric conditions. Accessory minerals include apatite, titanite, and Ti-magnetite. We propose that limestone assimilation followed by fractional crystallization are plausible dominant processes in the geochemical evolution of the Ambitle volcanics. Clinopyroxene fractionation is dominant in the mafic volcanics whereas hornblende fractionation is a major petrologic process within the intermediate suites proven by the enrichment of LREE and depletions in MREE and HREE. Feni magmas are also highly enriched in REEs relative to neighboring arcs. This study is globally significant as alkaline magmas are important sources of Cu, Au, and REE as critical elements for green energy and modern technology.

Keywords: Ambitle; Feni; TLTF; alkaline magmatism; hornblende; feldspathoid; REE



Citation: Ponyalou, O.L.; Petterson, M.G.; Espi, J.O. The Petrology and Geochemistry of REE-Enriched, Alkaline Volcanic Rocks of Ambitle Island, Feni Island Group, Papua New Guinea. *Geosciences* **2023**, *13*, 339. <https://doi.org/10.3390/geosciences13110339>

Academic Editors: Marco Viccaro and Jesus Martinez-Frias

Received: 13 June 2023

Revised: 2 October 2023

Accepted: 11 October 2023

Published: 6 November 2023



Copyright: © 2023 by the authors. Licensee MDPI, Basel, Switzerland. This article is an open access article distributed under the terms and conditions of the Creative Commons Attribution (CC BY) license (<https://creativecommons.org/licenses/by/4.0/>).

1. Introduction

The Feni Island Group is part of the Tabar–Lihir–Tanga–Feni (TLTF) alkaline volcanic chain within the New Ireland Basin (NIB), New Ireland Province (NIP), northeast Papua New Guinea (PNG). Our first paper [1], also published in this journal, presents an overview of the geological and tectonic evolution of PNG and Feni. NIP is made up of several islands: New Ireland, New Hanover, Mussau, Djaul, and the TLTF islands (Figure 1). The TLTF and NIB are bounded by New Ireland to the west and the older Kilinailau Trench (KT) to the east (Figure 1). The TLTF chain, KT, Bougainville, New Ireland, and New Britain

form the New Guinea Islands Terrane within the greater Melanesian Arc and are part of a series of arcs and trenches within the seismically and volcanically active SW Pacific region (Figure 1). Regional and location maps of the study area are presented in the first paper [1].

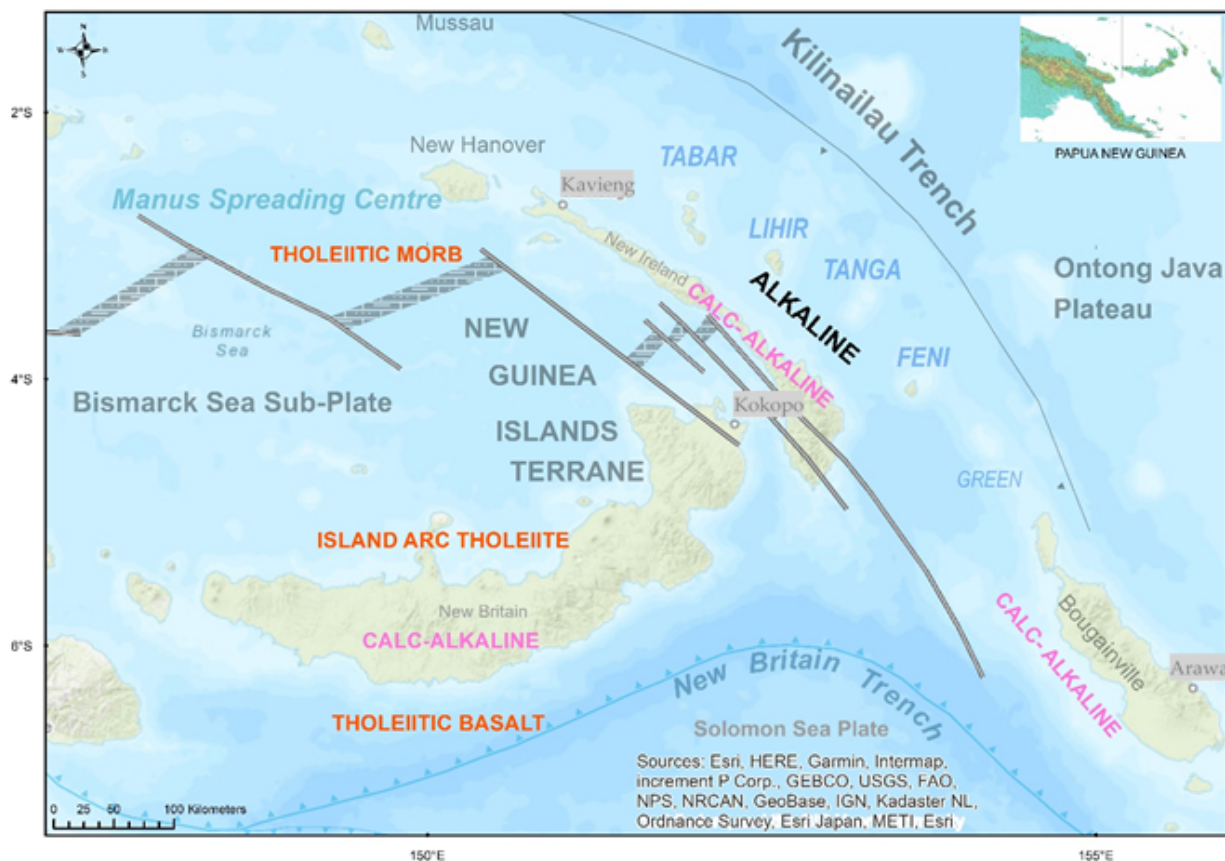


Figure 1. Regional tectonic setting of the alkaline Tabar–Lihir–Tanga–Feni island chain within the New Guinea Islands Terrane. Igneous geochemical classification of the various rock types and tectonic settings discussed in Ponyalou et al. [1] are highlighted.

Feni consists of Babase and Ambitle islands located between geographic coordinates $3^{\circ}45' S$, $153^{\circ}30' E$ and $4^{\circ}15' S$, $154^{\circ}00' E$, forming the southern end of the Pliocene to Holocene alkaline TLTF chain [1–3]. The TLTF chain hosts significant gold reserves associated with alkaline magmatism at Lihir (~23 Moz Au) and Simberi (~2.2 Moz Au) mines [4,5]. Recent papers by Lindley [6–8] and Brandl et al. [9] focus on the geology, mineral deposits, and geotectonic evolution of Feni and the TLTF, respectively.

The TLTF chain is proximal to two subduction zones: the older Kilinailau Trench directly east and the New Britain Trench (NBT) further south [1]. The geochemical patterns of the TLTF magmatic rocks indicate island arc signatures (i.e., high LILE and depleted HFSE) [2]. However, several authors attribute the formation of the TLTF to rifting associated with the opening of the Manus Basin ~3.5 Ma due to the fact that there is no seismically active slab under the TLTF [1,2]. Furthermore, the TLTF volcanism is relatively young and is not directly related to the older Eocene–Oligocene Kilinailau–Melanesian Arc subduction system. O’Kane [10] noted a slab tear on the down-going Solomon Slab at the curved New Britain Trench proximal to Feni. Given the tectonic complexities of the region, the general research question arises: how did the alkaline magmatic rocks of Feni form? The purpose of this study, therefore, is to (1) present and interpret the petrographic, mineralogical, and geochemical data from Ambitle, Feni, within the context of the tectonic evolution of the TLTF chain, and (2) propose a geodynamic, petrogenetic model for the Feni volcanic rocks in order to understand the processes that produced these rocks.

The Feni islands were initially targeted as a natural laboratory of Au-rich alkaline to calc-alkaline volcanism. Fieldwork included mapping the structural and geological units of Feni and sampling a representative suite of rocks for petrographic, mineralogical, and geochemical research [1]. Comparisons were also made with volcanics from neighboring arcs which include the Quaternary New Britain Arc, Manus back-arc basin, and Gallego in the Solomon Arc. The Gallego Volcanic Field (GVF) on Guadalcanal, Solomon Islands, was also visited in 2009 and sampled as it is an adjacent arc continuing on from the NW-trending Manus–Kilinaillau Trench.

2. Alkaline Magmatism in PNG

In addition to the TLTF chain, shoshonitic or alkaline rocks also occur in other parts of PNG. These include the Highlands (i.e., Porgera, Crater Mountain, Mt Hagen, Mt Giluwe), Oro (i.e., Mt Lamington pre-1951 volcanics), southeast Papuan Peninsula (i.e., Cloudy Bay Volcanics), and Milne Bay (i.e., Kutu Volcanics, Gabahusuhusu Syenite) and are also closely linked to gold mineralization [11–13]. Within the SW Pacific region, shoshonitic rocks also occur in North Fiji and the Lau back-arc basin [14,15], Sunda Arc in Indonesia, and Cadia in Australia [16]. Unlike the voluminous calc-alkaline porphyry Cu-Au magmas formed during subduction in island and magmatic arc settings, alkaline or shoshonitic magmas are formed post-subduction from low-degree partial melting of subduction-modified lithospheric mantle during extension [15,17]. Post-subduction processes include slab rollback, slab delamination, or slab tear [17,18].

Feni is a group of alkaline stratovolcanoes built on an Oligocene oolitic limestone basement [2]. Small outcrops of limestone and siltstone are noted on Ambitle and Babase islands (Figures 2 and 3) which appear to be older than the volcanics [1]. Miocene limestone units are also abundant on Simberi, New Ireland, and the New Ireland Basin. The emplacement of the volcanic and subvolcanic undersaturated, alkaline rocks of the TLTF are controlled by major NW extensional faults transected by later faults (Figures 2 and 3). On Ambitle, Cu-Au mineralization and geothermal activity are also constrained within the NW-trending Niffin Graben along intersections with later NE and NS faults [1].

Previous work published on the geology, alkaline magmatism, and porphyry–epithermal Cu-Au prospectivity of Ambitle includes Johnson et al. [18], Heming [19], Wallace et al. [2], and Licence et al. [20]. Heming [19] described the undersaturated lavas on Ambitle as basanite, tephrite, trachyte, and ankaramitic (or pyroxene-rich) lavas. He observed olivine, clinopyroxene, plagioclase, and hauyne within the basanite, whereas in the tephrite, amphibole and mica were dominant in the absence of olivine and hauyne. He also noted that the lavas contained unusually high concentrations of incompatible trace elements relative to island arc basalts and andesites. Heming [19] suggested that the undersaturated Ambitle lavas were most closely related to those from the Lesser Sunda Arc in Indonesia. Wallace et al. [2] described the rocks of Feni as alkali basalt, tephrite, basanite, phonolitic tephrite, tephritic phonolite, trachybasalt, trachyandesite, transitional basalt, and quartz–trachyte. The quartz–trachyte cumulodome is observed throughout the TLTF chain as the youngest and the most silica-saturated volcanic rock [2]. Wallace et al. [2] noted that most of the Ambitle volcanic geochemical signatures were typical of island arcs, including the high concentration of the incompatible large ion lithophile elements or LILE (i.e., Rb, Ba, Sr, K) relative to the high field strength elements (HFSE) and low Ti (which is generally high for most silica-undersaturated rocks from intercontinental arcs).

The outcropping rocks of Ambitle and Babase are mostly feldspathoid-bearing mafic to intermediate alkaline volcanics and subvolcanic rocks with rare quartz–trachydacite porphyries. Drilling in the Kabang prospect on Ambitle by past companies intersected a syenite porphyry intrusive with prospective porphyry–epithermal alteration and mineralization at depth [20]. Older company maps show a monzonite intrusive body at Matoff [21] but this was not visited during our field excursions (Figures 2 and 3).

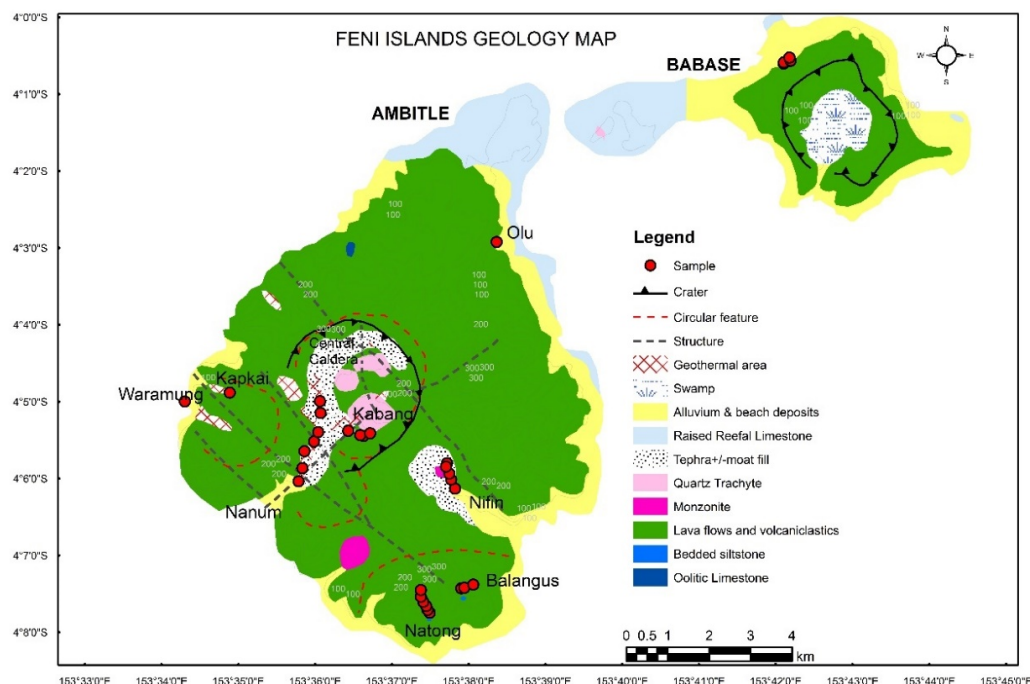


Figure 2. Geology and sample location map of Feni Island Group. Geology modified after Wallace et al. [2] and Esso [22] and includes our mapping and interpretations.

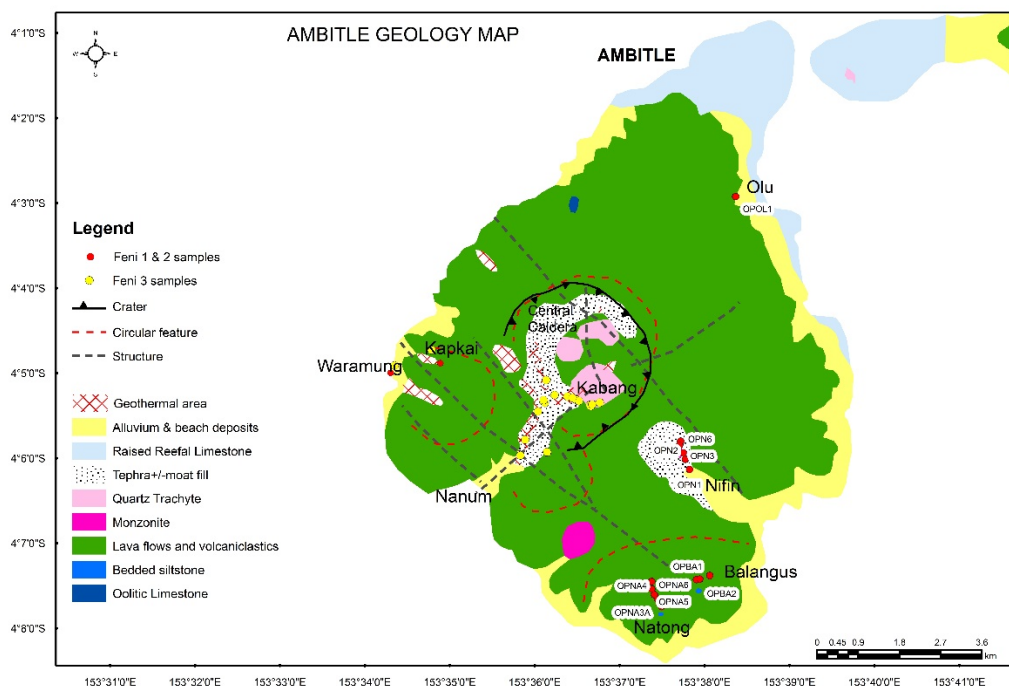


Figure 3. Geology map of Ambitle. Red circles represent samples collected for this study from the first two field trips. Sample IDs indicated for samples collected from outcrops. Yellow samples represent samples collected in the third field trip that were not analyzed.

3. Materials and Methods

Fifty-two (52) rock samples comprising twenty-one (21) float and thirty-one (31) outcrop samples were collected from Feni during two field trips in 2009 and labelled as Feni 1 and 2 (Figure 3). Several outcrops on Ambitle Island were mapped and sampled at the following localities: Natong, Niffin, Balangus, and Olu Creek (Figure 2). A third field trip (i.e., Feni 3) was carried out in January 2011 where outcrop samples were collected

from Nanum and Kabang on Ambitle (Figure 3) but these were not analyzed due to a lack of funding and limited time factor [23]. For the purpose of this paper, a representative suite has been selected for whole-rock geochemical data presentation. The full analytical data of all 52 samples are appended.

The samples collected were prepared and analyzed in PNG and the United Kingdom (UK). Thin sections and polished sections were prepared at the Earth Sciences Division (ESD) of the University of Papua New Guinea (UPNG) and the Geology Department of the University of Leicester (UOL) in the UK. The sample preparation and geochemical analytical techniques are described below. All rock samples, including a few with weathered surfaces, were crushed into rock powder using agate balls in a Retsch Planetary Mill at the UOL for whole-rock geochemical analysis.

The crushed material of the 31 samples (i.e., F1–36) from the Feni 1 trip were submitted to OMAC Laboratories Ltd. in Ireland for inductively coupled plasma mass spectrometry (ICP-MS) analysis of major and trace elements using the lithium borate fusion dissolution technique. Aqua regia dissolution was also applied on samples F1–36 for base and precious metal analysis. QAQC analyses of blanks, duplicates, and standards are included in the online Supplementary Information.

Twenty-three (23) samples (OPBA1-OPOL1) from the Feni 2 trip were analyzed for major and trace elements with the PANalytical Axios Advanced XRF X-ray fluorescence (XRF) spectrometer and PANalytical SuperQ software at the UOL Geology Department. The crushed samples were initially prepared into (1) a pressed powder pellet for trace element analysis and (2) a glass bead for major elemental analysis. The glass bead was made from the fusion of the rock powder with lithium metaborate or tetraborate. Instrument calibration and precision–accuracy measurements were conducted using various reference materials at the UOL Geology lab. Counting statistic errors are available within the raw XRF data spreadsheet under sheet “axrht322 cse”.

The left-over rock powder of the Feni 2 samples was also submitted to OMAC Laboratories for whole-rock geochemical and gold analysis. See Supplementary Data for all XRF and ICP MS results. The results were cleaned to exclude all weathered and altered igneous rocks and those possessing a loss on ignition (LOI) > 5% resulting in a total of 26 representative samples from Feni. Both the ICP-MS and XRF datasets were then used in the creation of bivariate plots, ratios, spider plots, and discrimination diagrams.

Electron microprobe analysis (EMPA) was conducted using the JEOL 8600 Superprobe at UOL for the determination of major elemental oxides in the polished sections of selected igneous rocks. Prior to analysis, the polished sections were coated with carbon to prevent ionization and the subsequent damage of minerals by the electron beam. The microprobe uses a wavelength dispersive system where a 30 nA current and a 15 kV accelerating voltage were used for all analyses. A 10 µm beam was employed for the analysis of feldspars and micas whilst a 5 µm beam was used for other minerals. Precision for electron probe analysis, calculated from counting statistics, was generally better than ±1% for measurements > 10 wt%, and better than ±5% for contents > 0.5 wt%. Trace element analysis of mineral phases cannot be carried out using the electron microprobe but is usually achieved via laser ablation ICP MS (LA ICP MS) and secondary ion mass spectrometry (SIMS).

The composition for each mineral phase was then calculated from the electron microprobe analysis using appropriate conversion spreadsheets. Olivine composition (Te, Fa, Fo, Ca-Ol) was calculated from Mineral Formulae Recalculation (carleton.edu). Pyroxene compositions were calculated in the PYXCALC spreadsheet from Gabbrosoft. Olivine and pyroxene compositions were then plotted in ternary diagrams online (Ternary Plot Generator—Quickly create ternary diagrams). Amphibole classification was carried out using the Ca-amphibole classification scheme by Leake et al. [24] and the AMPH13 spreadsheet by Gabbrosoft.org for stoichiometric calculations of electron microprobe analysis (<https://www.gabbrosoft.org/wp-content/uploads/2018/07/AMPH13.xls>) accessed on 19 June 2022. The AMP_TB excel spreadsheet published by Ridolfi et al. [25] was also utilized to interpret amphibole composition, pressure, temperature, and depth of formation.

4. Results

The results of this study are presented according to field or outcrop observations (Figures 2 and 3) as summarized in our first paper [1], total alkali vs. silica (TAS) volcanic rock classification plots, petrography, mineral chemistry, and whole-rock geochemistry. Mineral chemistry and microscopic petrography are complementary to each other. The whole-rock geochemistry section is further subdivided into major elements, trace elements, and rare earth elements (REE). Trace element data are also used to produce tectono-discrimination diagrams and prospectivity or Cu-Au fertility plots. The Feni geochemical data are compared with the volcanic and intrusive rocks from the Gallego Volcanic Field (GVF) in Guadalcanal, Solomon Islands sampled by the same authors in 2009 and previously published by Petterson et al. [26]. Comparisons are also made with rocks from nearby arcs such as the Manus Spreading Centre (MSC) and the New Britain Arc using published data by Woodhead et al. [27].

4.1. Alkali vs. Silica Volcanic Rock Classification

The Feni volcanic rocks are mainly high K, shoshonitic or alkaline in chemistry and include basalt, trachybasalt, trachyandesite, phonotephrite, and trachydacite (Figure 4). The Feni rocks are colored black and labelled as TLTF in the TAS plot (Figure 4) with SiO_2 values ranging between 45% and 67% and $\text{K}_2\text{O} + \text{Na}_2\text{O}$ values falling between 3% and 12%. In comparison, Gallego rocks in the Solomon arc are mainly calc-alkaline andesite and basaltic andesite with minor gabbro (plotting in the basalt field in Figure 4). Data from the New Britain Quaternary volcanic arc (labelled NBT for New Britain Trench), Solomon Slab Basalt (from the sea floor that is subducting at the New Britain Trench), and the Manus MORB were adopted from Woodhead et al. [27] and plotted for comparison (Figures 1 and 4). The Manus MORB is largely tholeiitic whilst the New Britain arc and the Solomon Slab are mainly low K island arc tholeiites [27]. Some rocks from New Britain are also calc-alkaline. The geochemical classification resulting from Figure 4 is shown spatially on the regional map in Figure 1.

4.2. Petrography and Mineral Chemistry

The volcanic rocks of Feni are generally recognized as either primitive or evolved. The primitive suites are the mafic or basic volcanics which include basalt (F4, F7, F11, F15, F16, F19, OPN6, OPN7, OPN8A, and OPOL1), trachybasalt (F2, F5, F8, F17, and OPBA1), and mafic phonotephrite (OPN3). The evolved rocks include the intermediate and felsic porphyritic suites. The intermediate units include the trachyandesite porphyries from Natong (OPNA1, OPNA3A, OPNA3B, OPNA4, and OPNA5) and an evolved phonotephrite from Niffin (OPN8B). The felsic magmas are the trachydacite porphyries (F12, F33). Phonotephrite has two variants: a mafic, fine-grained grey black unit (OPN3) and a grey, porphyritic, hornblende-bearing unit (OPN8B).

Figure 5 shows the modal abundance of minerals observed in thin section from the mafic, intermediate, and felsic units on Feni. The primitive basaltic and fine-grained phonotephrite magmas contain feldspathoids, alkali feldspars, clinopyroxene, and minor olivine (Figures 5–7). Feldspathoid minerals, mainly leucite and nepheline, are observed in the basalt, trachybasalt, and the mafic or more primitive phonotephrite samples (i.e., OPN3, OPN8A). Nosean was potentially noted in the Natong trachyandesite. Hornblende occurs in trachyandesite and the evolved phonotephrite from Natong and Niffin, respectively (Figure 5). Biotite is most abundant in the felsic trachydacite porphyry but also occurs minimally in the trachyandesite and the hornblende-bearing phonotephrite almost as an accessory mineral (Figure 5). Remnant clinopyroxene appears to have been replaced by hornblende in the trachyandesite and phonotephrite samples. Apatite is present throughout all rock types but is most abundant in the hornblende-bearing trachyandesite at Natong and the evolved hornblende–phonotephrite at Niffin. Apatite abundance is strongly associated with hornblende clusters (Figure 5).

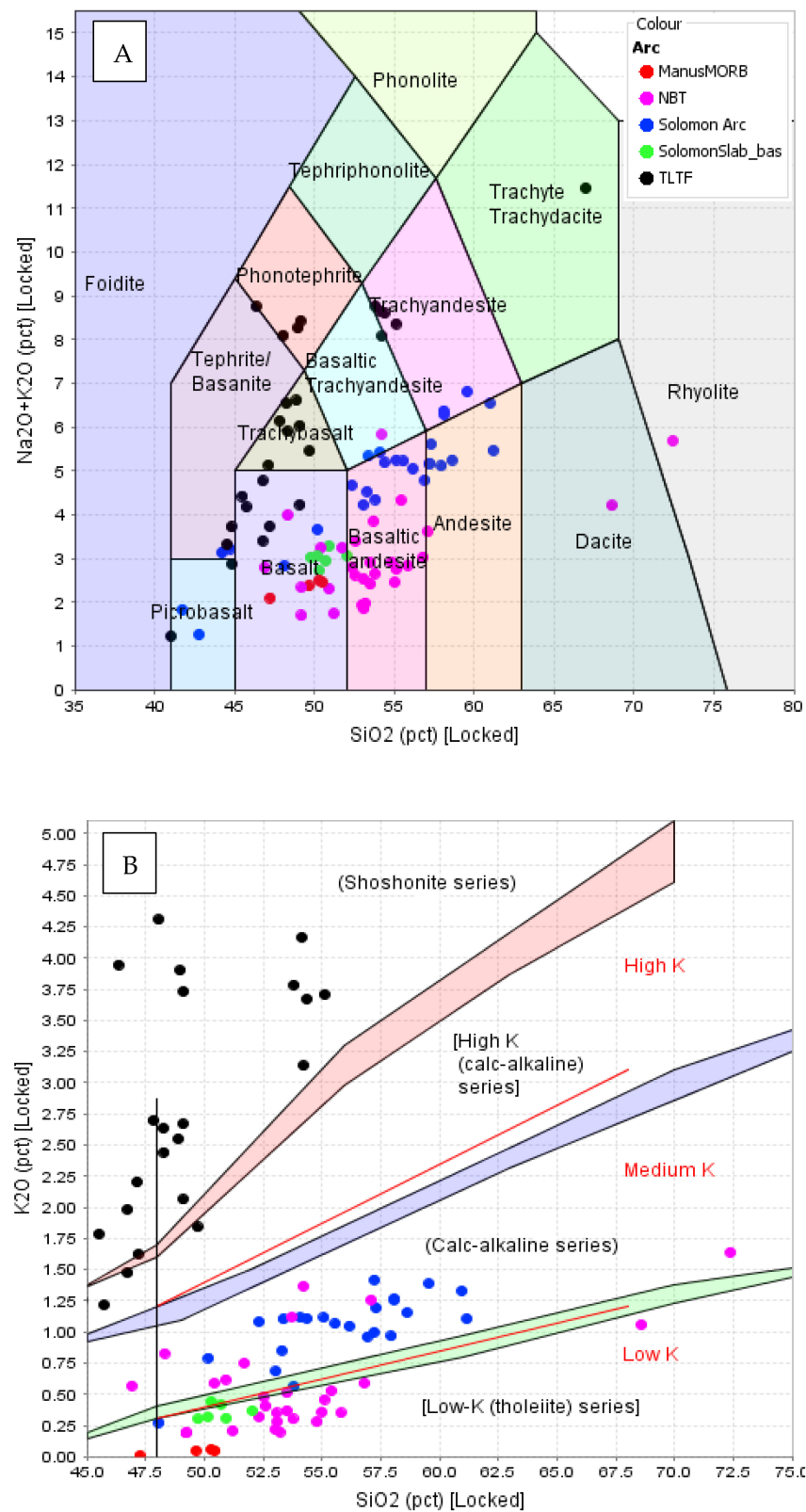


Figure 4. (A) TAS classification diagram after Le Maitre et al. [28] and (B) subdivision of subalkalic rocks using K_2O vs. SiO_2 [29] of Feni (black circles), Gallego (blue circles), New Britain (pink), Solomon Slab (green), and Manus MORB (red). NBT and Manus MORB data were obtained from Woodhead et al. [27] with permission. Plots were made in the IOGAS software.

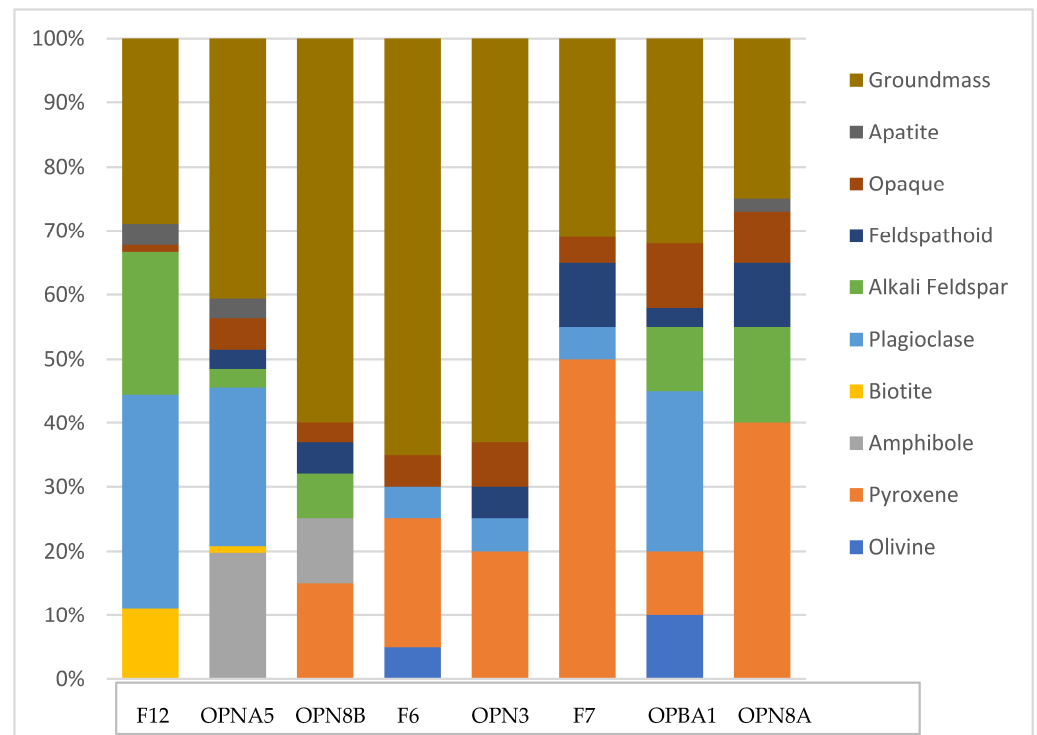


Figure 5. Modal abundance of minerals observed in thin section, as determined from gridding of thin section scans (minimum 200 points). Samples are ordered from felsic to mafic from left to right. F12 is trachydacite. OPNA5 is hornblende trachyandesite. OPN8B is the porphyritic hornblende-phonotephrite. F6 and OPN3 are mafic phonotephrite samples. Basalt samples are F7, OPBA1, and OPN8A. Note the abundance of pyroxene or clinopyroxene in the mafic suites at the expense of olivine.

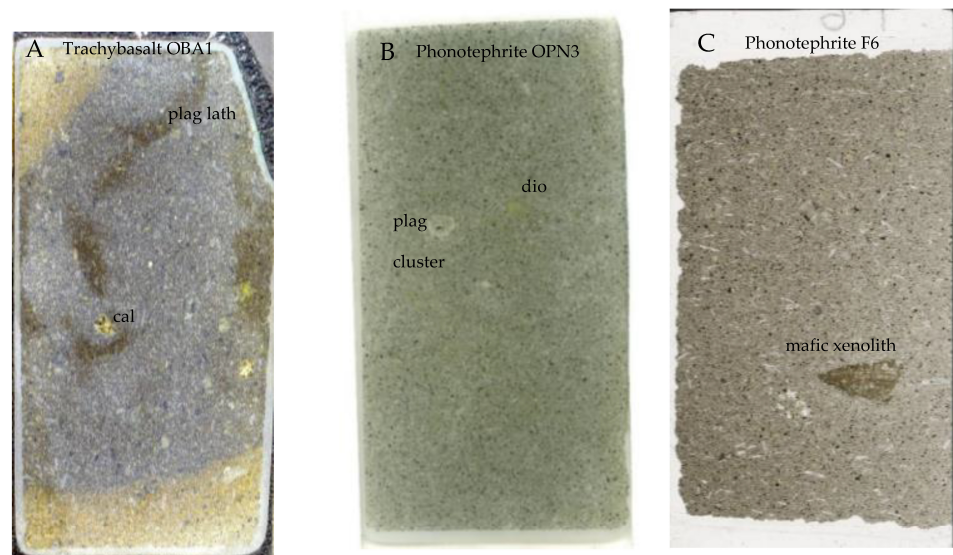


Figure 6. Polished thin section scans of mafic volcanic rocks from Ambitle. (A) OPBA1 trachybasalt from Balangus. The trachytic alignment of plagioclase (plag) laths are notable. Secondary calcite (cal) is also present. (B) OPN3 is the aphanitic, grey phonotephrite outcrop sample from Niffin. Green diopside xenocryst (dio) and plagioclase (plag) cluster are indicated. (C) F6 phonotephrite float sample with trachytic alignment of plagioclase laths and a triangular-shaped mafic xenolith.

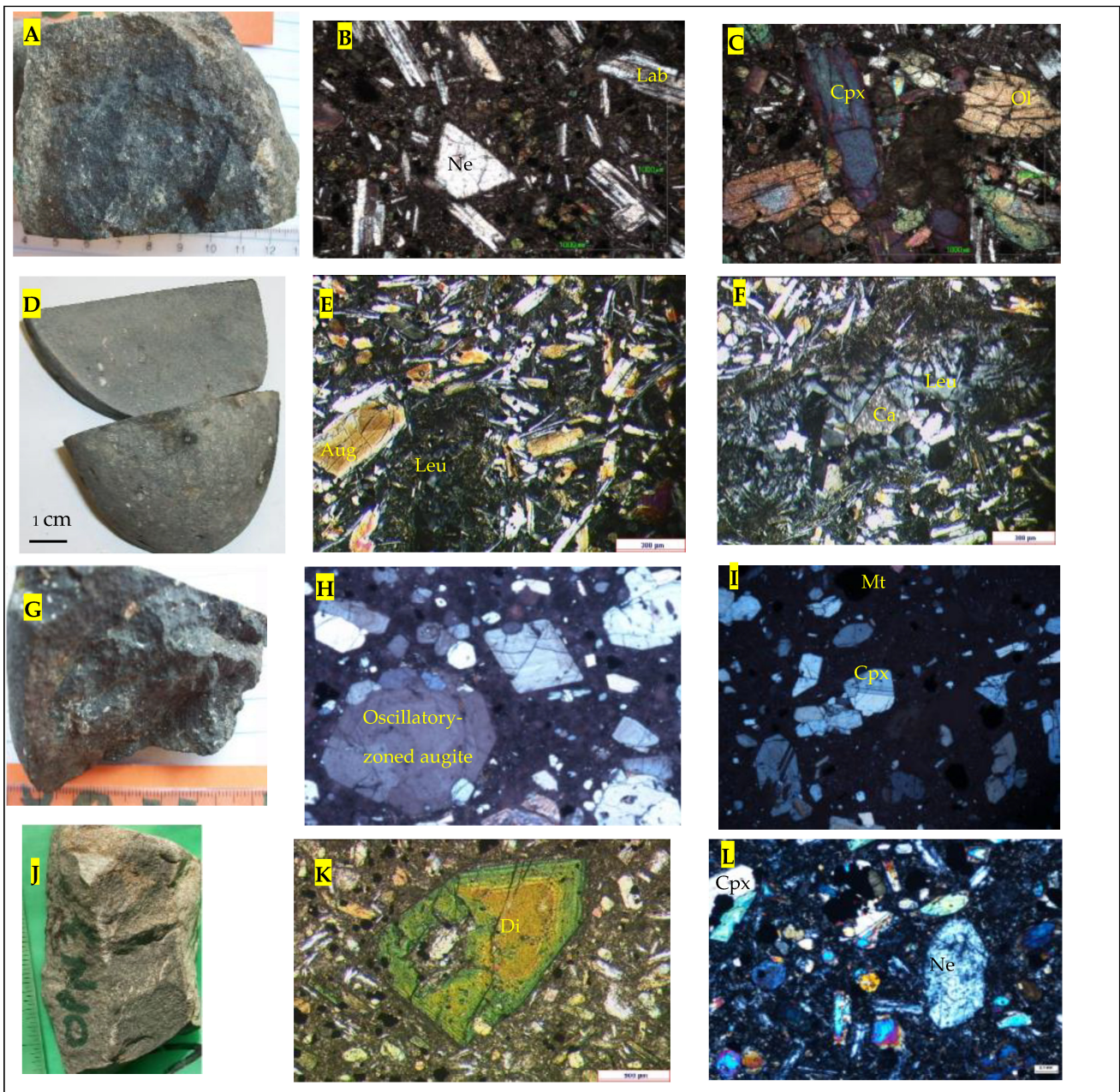


Figure 7. Hand specimen and photomicrographs of basaltic rocks. (A) Trachybasalt OPBA1 from Balangus, eastern Ambitle. (B) Euhedral nepheline surrounded by labradorites (Lab) oriented in a trachytic flow texture (xpl), OPBA1. (C) Clinopyroxene (Cpx) and olivine (Ol) glomerocryst under xpl, OPBA1. (D) Aphanitic basalt F7 hand specimen with calcite amygdales. (E) Rectangular augite (Aug) crystal 0.35 mm with hour-glass extinction in xpl (mid-left), F7. Note needle-like laths of plagioclase and second-order yellow-pink augite grains. (F) Amygdalar calcite (Cal) in between leucite (Leu) grains exhibiting radial and complex twinning under xpl. Basalt F7. (G) OPN8A pillow basalt from Niffin with calcite amygdales. (H) Oscillatory-zoned augite in pyroxene–phyric basalt OPN8A. Scale is the same as K. (I) Exsolution lamellae in clinopyroxene (Cpx). Titanomagnetite (Mt) associated with cpx, OPN8A. Scale is the same as K. (J) Phonotephrite OPN3 sample from Niffin. (K) Zoned diopside (Di) megacryst under XPL, OPN3. Refer to electron microprobe analysis of this crystal under clinopyroxene mineral chemistry. (L) OPN3 photomicrograph of numerous clinopyroxene crystals and a nepheline (Ne) crystal.

4.2.1. Mafic Volcanic Lava Suite

The mafic volcanic suite includes basalt, trachybasalt, and phonotephrite (Figure 6). Mafic volcanic rocks are mainly aphanitic or fine-grained, vesicular, amygdaloidal, and microporphyritic in texture, with minor glass in the matrix. Clinopyroxene, particularly augite, is the essential mineral phase observed in thin section with minor or no olivine. These ferromagnesian minerals occur as phenocrysts (1–3 mm), microphenocrysts (<1 mm), and glomerocrysts (2–4 mm) and rarely as xenocryst (>4 mm) in a finer matrix of the same composition. Other essential minerals include plagioclase and feldspathoid, followed by titanomagnetite and apatite as accessory minerals. Secondary minerals that form after the alteration of feldspars or that infill vesicles include clay, calcite, and zeolite. The basaltic rocks sampled in this study are dominated by clinopyroxene but a few contain olivine crystals and xenocrysts that are interpreted to be from the lower parts of the mantle.

Olivine–Clinopyroxene Basalt

Olivine–clinopyroxene-bearing basalt samples include F5, F11, and OPN7. OPN7, sampled from a Niffin basalt outcrop, is dominated by diopside followed by minor forsteritic olivine with magnesium-rich cores (as determined by the electron microprobe). F11 consists of euhedral clinopyroxene megacrysts up to 15 mm in length within a groundmass of smaller fractured fragments and lesser altered olivine grains pseudomorphed or coated by an oxide mineral.

Trachybasalt OPBA1 (Figures 6A and 7A) is another olivine–clinopyroxene-bearing basaltic rock sampled from a massive lava flow at Balangus Creek, eastern Ambitle. It is melanocratic, fine-grained, or microcrystalline with flow-oriented plagioclase grains, and abundant mafic lath-shaped clinopyroxene crystals in hand specimen. OPBA1 exhibits a seriate texture under the microscope (Figure 7B,C). The modal mineral composition is plagioclase (20%); sanidine (15%); olivine (~10%); clinopyroxene (20–30%); accessory oxides (~15%); and minor nepheline (~10%) set in a fine-grained matrix of similar composition. The plagioclase phases include labradorite laths exhibiting multiple twinning and tabular anorthite with compositional zoning. In Figure 7B, a euhedral nepheline crystal is surrounded by labradorites oriented in a trachytic flow texture. Sanidine grains are flow-oriented and diagnostically simple-twinned. A clinopyroxene–olivine glomerocryst is observed microscopically (Figure 7C) and in hand specimen. The subhedral round and elongated olivine crystals lack cleavage and typically display curved fractures.

Clinopyroxene Basalt

F7 is a microporphyritic basaltic sample with secondary calcite amygdalae in hand specimen (Figure 7D). In the thin section, F7 essentially comprises augite (30%) and acicular plagioclase intergrowths (35%) with minor leucite (~15%) and secondary calcite amygdalae (~5%) in a fine matrix of the same composition (~10%). A rectangular or prismatic augite crystal (0.35 mm long) exhibits hour-glass extinction and good partings (Figure 7E, mid-left) surrounded by needle-like laths of plagioclase and second-order yellow-pink augite grains in F7. Other major minerals include plagioclase (i.e., andesine), alkali feldspar (i.e., sanidine), feldspathoid, and accessory magnetite. The feldspathoid minerals observed in the thin section were nepheline and leucite. The leucite grains (Figure 7F) exhibit diagnostic radial and complex twinning under crossed polars with amygdalar calcite in between. Secondary minerals include clay, calcite (Figure 7D,F), and zeolite.

OPN8A is sampled from a pillow basalt outcrop along a westerly tributary of the Niffin River. It is a melanocratic, aphanitic, and pyroxene–phyric basalt with secondary calcite amygdalae (~5%) on the surface (Figure 7G). In the thin section, the dominant phenocryst phase is clinopyroxene (augite) ~45–50% followed by feldspathoids and the opaque magnetite set in a fine-grained matrix of similar mineralogy. This basalt is devoid of plagioclase, olivine, or amphibole minerals. Augite phenocrysts occur as euhedral prisms and tabular, eight-sided oscillatory-zoned crystals sometimes with exsolution lamellae,

surface fractures, and perfect cleavage (Figure 7H,I). Microphenocrysts of clinopyroxene display hour-glass extinction and Carlsbad twinning.

Pyroxene-Olivine Phonotephrite

Phonotephrite (Figure 7J) is a medium to light grey, fine-grained volcanic rock consisting of olivine, pyroxene, plagioclase, and feldspathoid in the more primitive mafic samples, whereas in the evolved units, the texture is porphyritic and contains hornblende and minor pyroxene (without olivine). Phonotephrite samples include cobble floats from Waramung Beach (F6, F9) and outcrop samples (OPN3, OPN8B) from the Niffin area. Two varieties are recognized: olivine-pyroxene phonotephrite (OPN3, F6) and hornblende–clinopyroxene phonotephrite (OPN8B). Figure 7K shows a zoned clinopyroxene (diopside) megacryst that was also analyzed in the electron microprobe at UOL. Clinopyroxene and nepheline phenocrysts are observed in Figure 7L.

4.2.2. Intermediate and Felsic Subvolcanic Suite

The intermediate and felsic subvolcanic or hypabyssal intrusive rocks include the evolved phonotephrite, trachyandesite, and trachydacite. These rocks are medium-grained and mainly equigranular or porphyritic in texture (Figure 8). The main phenocryst phases are plagioclase, feldspar, and hornblende. Accessory apatite crystals are also observed in the trachyandesite and trachydacite.

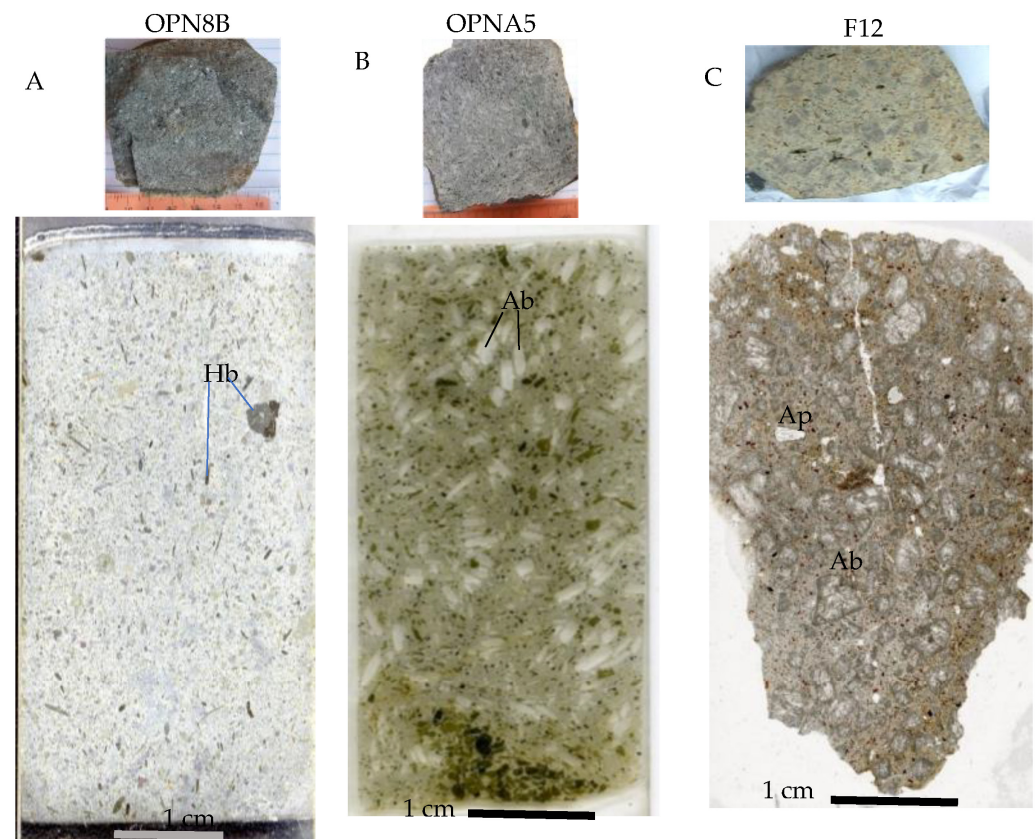


Figure 8. Polished thin section scans and hand specimens of intermediate and felsic subvolcanic rocks from Ambitle. (A) Hornblende–phyric phonotephrite OPN8B sampled from outcrop in Niffin. (B) Hornblende trachyandesite porphyry OPNA5 from outcrop in Natong. (C) Trachydacite porphyry (float) F12 from Waramung Beach that may have come from the quartz–trachyte cumulodomes in the Central Caldera area. Hb = hornblende, Ab = albite, Ap = apatite.

Clinopyroxene-Hornblende Phonotephrite

OPN8B is a light-grey, mesocratic, slightly weathered porphyritic phonotephrite consisting of hornblende laths (5%), clinopyroxene (10%), feldspathoid (3%), and alkali feldspar (3%) phenocrysts set in a finer grained, light grey matrix (Figures 8A and 9A–C). Two types of clinopyroxene were observed optically. The euhedral clinopyroxene is eight-sided in the basal section and exhibits third-order yellow and pink interference colors (Figure 9A). Anhedral clinopyroxene grains, which are rare occurrences, appear to have been remelted or corroded on the edges and exhibit third-order blue and purple birefringence, inclined extinction, good cleavage, and occasional exsolution lamellae (Figure 9B). These clinopyroxenes appear to experience some degree of amphibole alteration or replacement. Hornblende occurs as spindle-shaped laths, diamond-shaped grains, and coarse-grained megacryst (>2.5 mm) that are sometimes simple-twinned (Figure 9C). Sanidine or orthoclase is diagnostically simple twinned with low-order grey and white birefringence. Minor or rare anhedral feldspathoid is also present. Rare biotite inclusions were also noted in hornblende megacrysts.

Hornblende Trachyandesite

Trachyandesite (Figure 8B) is an intermediate, grey subvolcanic or hypabyssal intrusive rock of porphyritic, equigranular, sub-porphyritic, and trachytic texture mainly occurring as outcrops along Natong Creek. Primary minerals are hornblende (20 vol%) and albite (25%) phenocrysts with the occasional remnant pyroxene 5–10% (being altered to amphibole and chlorite), alkali feldspar, and hauyne ranging from 2 to 4 mm in grain size, and set in a groundmass of variable alteration (Figure 9D–I). Hornblende crystals form clusters or glomerocrysts (Figure 9G–I). Apatite (3%) appears to form euhedral crystals interstitially between the hornblende clusters or glomerocryst. Other accessory minerals include magnetite and titanite. Smectite clay, chlorite, and epidote alteration are common in propylitic-altered portions of the outcrop whilst fault-controlled quartz–clay–pyrite veins were observed in the field. The albite crystals are mainly tabular or prismatic, multi-twinned, and sometimes oscillatory zoned. Plagioclase laths may also assume flow orientation as seen in the trachytic texture. Mineral impingement and embayment are observed in some plagioclase crystals and indicate high energy and mechanical movement during magma flow. The hornblende is determined as magnesiohastingsite [24,25] via electron microprobe analysis and is discussed under the amphibole mineral chemistry section.

Biotite Trachydacite

The feldspar-biotite trachydacite (F12, F33) is a pinkish-white, leucocratic, crowded porphyry containing coarse cumulate K-feldspar and albite phenocrysts (~40 vol%) ranging from 2–5 mm, minor biotite microcrystals (0.2–0.6 mm), and accessory apatite (3 mm) set in a white, quartz–albite–sericite–clay–altered groundmass (Figure 8C). The source outcrop is inferred to be in the centre or south of Ambitle Island. In thin section, the crowded porphyry comprises albite (30%), K-feldspar-perthite pseudomorph (10%), alkali feldspar (10%), biotite (10%), opaque minerals (2%), hydrothermal quartz (2%), accessory apatite (1–3%), and trace pyrite (0.1%) in a silica–sericite–clay–altered groundmass (Figure 9J–L). The main cumulate phases are albite and alkali feldspar with overprinting cloudy sericite clay and cancrinite alteration (Figure 9J). Cancrinite is colorless under PPL but exhibits highly birefringent blues under XPL. Brown and strongly pleochroic biotite laths occur in the matrix as microcrystals (<1 mm) oriented in all directions (Figure 9J). The igneous biotite is partially replaced by phlogopite potentially indicative of a weak potassic alteration phase crosscut by late hydrothermal quartz as micro-veinlets. Hydrothermal alteration of mica is confirmed in the EMPA results where all biotite crystals analyzed are phlogopite (see mica mineral chemistry section). Fine-grained disseminated pyrite (0.1%) is associated with the late argillic alteration (silica–clay–pyrite) overprinting the weak potassic alteration. Feldspar phenocrysts occur as square and hexagonal euhedral crystals that are sometimes simple-twinned (Figure 9K). Albite occurs together with K-feldspar or perthite

distinguished by perthitic twinning. Accessory apatite (~1%) is colorless, prismatic, and has high relief with low birefringence (Figure 9L). Mineral analysis of this apatite grain is shown in Table 4. Opaque minerals, possibly iron, and titanium oxide, make up <2% of the rock.

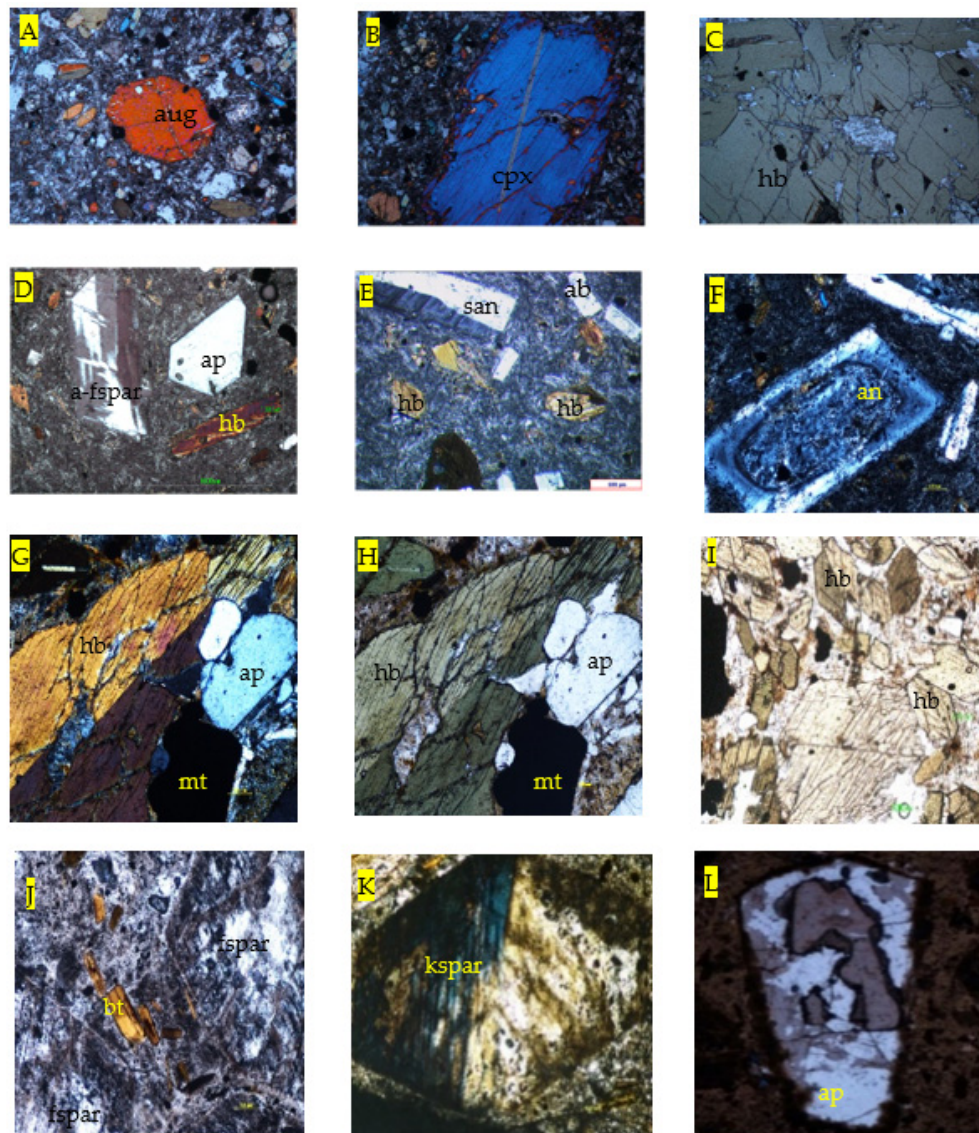


Figure 9. Thin section photomicrographs of evolved crustal rocks from Ambitle Island: phonotephrite OPN8B from Niffin (A–C), hornblende–feldspar trachyandesite porphyry OPNA5 from Natong (D–I), and biotite–feldspar trachydacite porphyry F12 (float) from Waramung Beach (J–L). (A) Eight-sided augite (aug) crystal surrounded by amphibole and clinopyroxene microcrystals and opaques, OPN8B, FOV 2.1 mm, XPL view. (B) Corroded clinopyroxene (cpx) megacryst with exsolution lamellae, OPN8B, FOV 2.1 mm, XPL view. (C) Hornblende (hb) megacryst, OPN8B, FOV 2.1 mm, PPL view. (D) Perthitic alkali feldspar (a-fspar), euhedral apatite (ap), and hornblende lath, OPNA5. (E) Simple-twinned sanidine (san), hornblende (hb), and smaller albite (ab) grains, OPNA5. (F) Zoned anorthite (an) in OPNA5 under XPL. (G) XPL and (H) PPL images of coarse, twinned hornblende crystal, smaller apatite grains, and Ti-magnetite as opaques (mt) in glomerocryst within OPNA5. (I) PPL image of numerous hornblende crystals with diagnostic diamond shape and intersecting inclined cleavages, OPNA5. Titanite is also present. (J) PPL view of sericite clay-altered cumulate hexagonal albite (fspar) crystals ~4–5 mm and smaller biotite (bt) ~0.5 mm grains in trachydacite sample F12. (K) Simple-twinned K-feldspar (kspar) ~ 4 mm long, F12. (L) Apatite grain (3 mm) in sample F12. EMPA analysis in Table 4.

Olivine Mineral Chemistry

Olivine occurs as minor phenocrysts and xenocrysts (<10 vol%) in some basalt and trachybasalt. Electron microprobe analysis was conducted on olivine crystals in a basalt in situ sample OPN7 from Niffin and a float basalt sample F5 from Ambitle Island (Figure 10). The olivine xenocryst in OPN7 is forsteritic in composition (Table 1, Figure 10), displaying a negative linear trend for CaO and a positive correlation with NiO (Figure 11). Olivine composition in OPN7 (Table 1) varied from Fo₈₇ to Fo₉₄ [Fo = 100 × molar Mg/(Mg + Fe)], Mg# 88–93 with a NiO content of 0.10 to 0.32 wt % (or 778–2546 ppm), and CaO content of 0.06 to 0.38 wt %. Basalt sample F5 also contains olivine crystals but are of lower forsteritic composition than OPN7 at Fo₈₂ to Fo₈₄ and Mg# 82.9–84.3 (Figure 10).

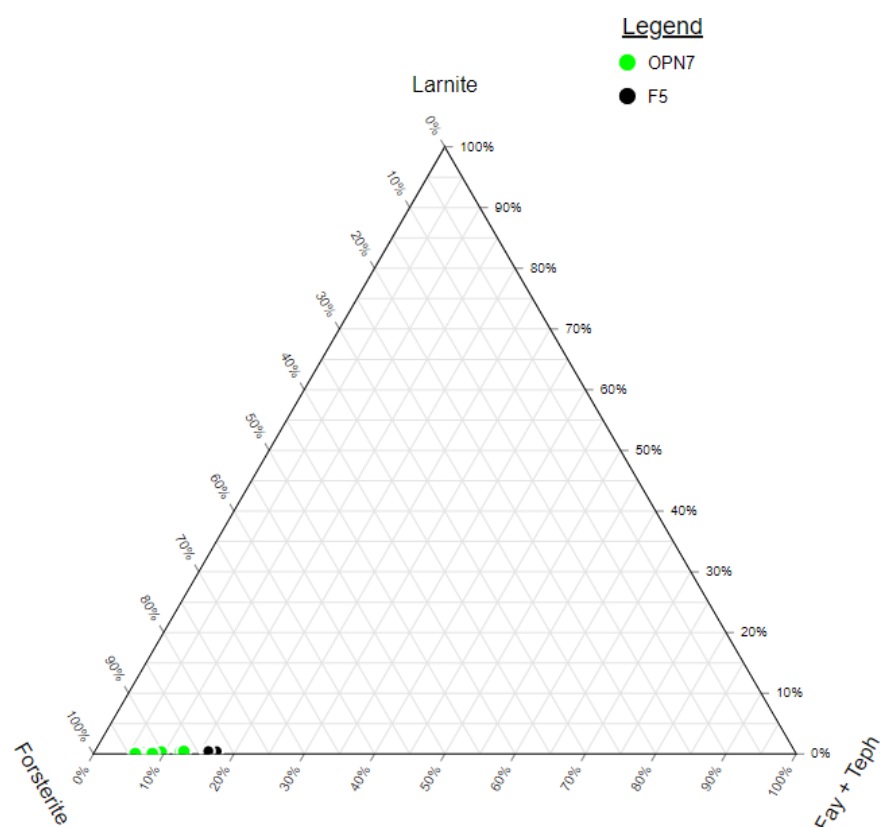


Figure 10. Ternary plot of olivine crystals from basalt sample OPN7 and F5 showing mainly forsterite (Mg_2SiO_4) composition. OPN7 is more forsteritic or magnesium rich than F5. Fay + Teph is short for Fayalite + Tephroite ($\text{Fe}_2\text{SiO}_4 + \text{Mn}_2\text{SiO}_4$). EMPA data plotted in www.ternaryplot.com accessed on 3 April 2022.

Table 1. Electron microprobe analyses for olivine in basalt sample OPN7.

Sample	OPN7	OPN7	OPN7	OPN7
Point	12	13	14	59
Job	emc02	emc02	emc02	emc02
SiO ₂ wt%	40.01	41.86	39.88	41.30
Cr ₂ O ₃ wt%	0.10	0.06	0.00	0.07
FeO wt%	6.90	7.00	10.78	6.79

Table 1. *Cont.*

Sample	OPN7	OPN7	OPN7	OPN7
MnO wt%	0.06	0.10	0.55	0.14
MgO wt%	50.19	50.42	45.58	51.63
CaO wt%	0.10	0.07	0.30	0.06
NiO wt%	0.29	0.27	0.10	0.32
Total	97.64	99.79	97.20	100.32
Ni (ppm)	2278.82	2145.234	777.942	2545.992
Mg#	93	93	88	93
Te (mole%)	0.061	0.000	0.601296	0.110
Fo (mole%)	92.6	93.8	87.4	94.02
Fa (mole%)	7.146	6.105	11.5952	5.8
Ca-Ol (mole%)	0.127	0.079	0.414751	0.071

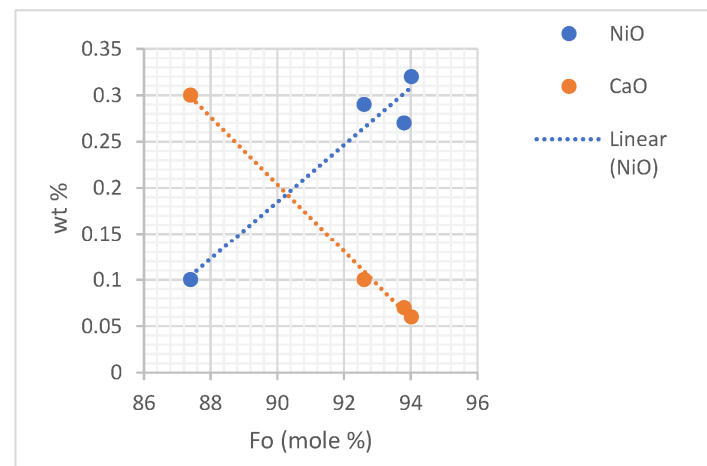


Figure 11. NiO and CaO (wt%) vs. Forsterite or Fo (mole%) in olivine in basalt OPN7. NiO positively correlates with forsterite. CaO decreases as Fo composition increases.

Clinopyroxene Mineral Chemistry

The mafic alkaline volcanic rocks of Feni are rich in clinopyroxenes, accompanied by feldspathoids, Fe-Ti oxides, and minor olivine. Electron microprobe analysis was conducted on a sector-zoned clinopyroxene xenocryst (Figures 6B and 7K) in the phonotephrite sample OPN3 from Niffin (Figures 12 and 13). Using the Ca-Mg-Fe quadrilateral ternary plot, the zoned pyroxene grain was classified as diopside ($\text{MgCaSi}_2\text{O}_6$) in Figure 13. It showed increasing MgO and CaO composition from rim to core but decreasing values of MnO, Al_2O_3 , FeO, and TiO_2 . The OPN8B phonotephrite sample also contains diopside phenocrysts. The diopside in the mafic phonotephrite OPN3 is more calcic than those in the mesocratic hornblende-bearing phonotephrite OPN8B.

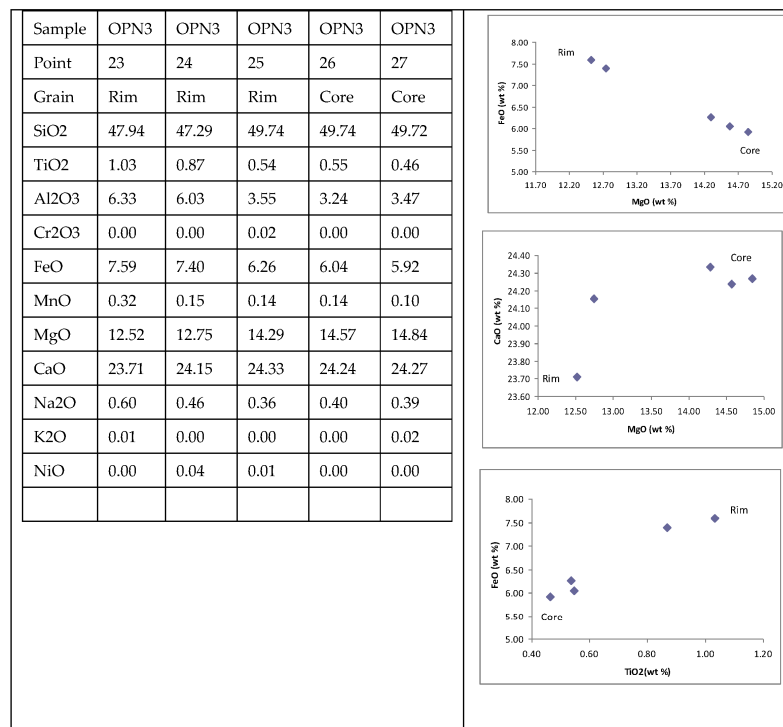


Figure 12. Tabulated analyses of zoned clinopyroxene in phonotephrite OPN3 and bivariate graphs of FeO vs. MgO, CaO vs. MgO, and FeO vs. TiO₂ to show compositional variations from core to rim. Core is rich in CaO and MgO whilst the rims are enriched in TiO₂ and FeO.

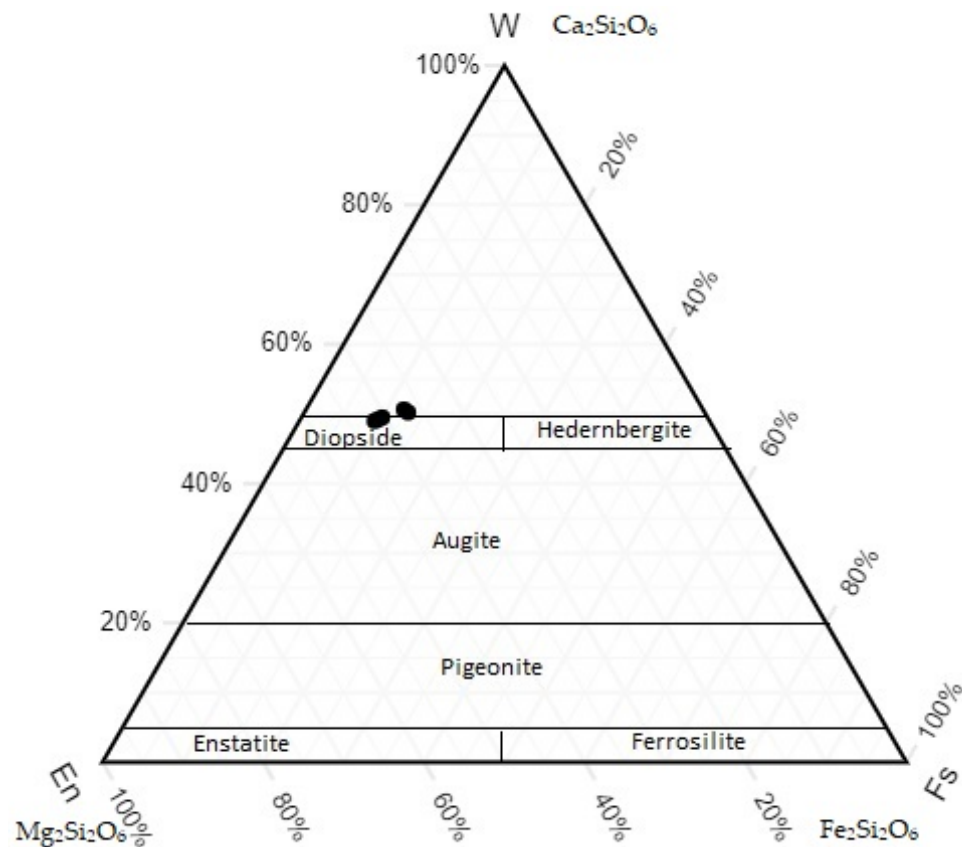


Figure 13. Ternary plot of clinopyroxene compositions from phonotephrite samples OPN3 and OPN8B. Mineral compositions calculated with PYXCALC from Gabbrosoft and plotted in Ternary Plot Generator—Quickly create ternary diagrams.

Feldspar Plagioclase Mineral Chemistry

Alkali feldspar and plagioclase are ubiquitous in both anhydrous mafic magmas and evolved hydrous magmas at varying proportions. Feldspathoids such as leucite and nepheline are distinguishable in thin section petrography but may become mixed up with alkali feldspar in mineral chemistry analyses. The olivine–clinopyroxene-bearing basalt and trachybasalt mafic suites are dominated by calcic labradorite, anorthites, leucite, and nepheline. Clinopyroxene-rich basalt and mafic fine-grained phonotephrite that are devoid of olivine usually contain nepheline, minor plagioclase, and alkali feldspar. The intermediate hornblende-bearing phonotephrite and trachyandesite porphyries, however, contain twinned albite, andesine, and labradorite cores within concentric zoned plagioclase crystals. In the biotite-quartz trachydacite, albite crystals predominate with perthitic twinning and orthoclase anti-perthites observed optically and under the electron microprobe. All EMPA analysis of feldspar and plagioclase are attached in the Supplementary Information.

A ternary plot of feldspar–plagioclase composition of selected samples is shown in Figure 14. Mafic phonotephrite sample F6 (Figure 14) contains oligoclase, andesine, alkali feldspar (Or_{35-53}), and nepheline [30]. The plagioclase crystals in the hornblende–phonotephrite sample F9 are mainly andesine (An_{30-50}) with minor oligoclase (An_{10-30}) and labradorite (An_{50-70}). The mafic phenocrysts in F9 are mainly hornblende and pyroxene. The plagioclase crystals in the Niffin phonotephrite sample OPN8B are mostly labradorite (An_{50-70}) with occasional albite (An_{0-10} or Ab_{99}) occurring alongside hornblende and pyroxene phenocrysts.

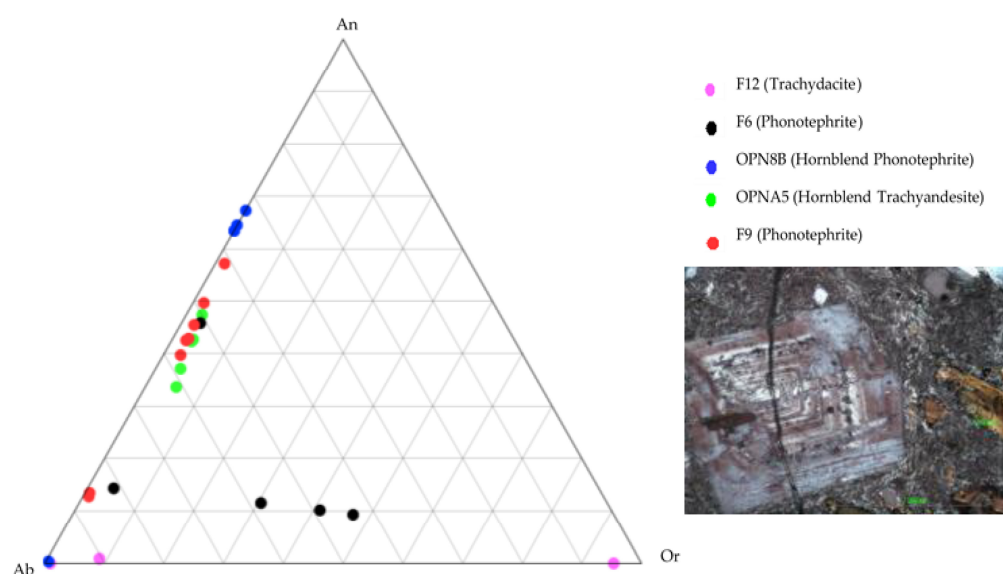


Figure 14. Ternary plot of feldspar–plagioclase compositions of selected samples (F12, F6, OPN8B, OPNA5, and F9) plotted in IOGAS. Each triangle represents 10 mol%. Insert: zoned tabular plagioclase in OPNA5 with albitic rims and anorthitic core.

In the Natong trachyandesite, the plagioclase phenocrysts include andesine (An_{30-50}) and labradorite (An_{50-70}) (Figure 14). An oscillatory-zoned plagioclase in OPNA5 showed cyclic compositional variations between sodium and calcium calculated at Ab_{46-61} or An_{37-47} . Zoned plagioclase crystals have sodic rims of andesine composition and a calcic core of labradorite composition (An_{52}). Crystal fractionation and slow cooling are most likely responsible for the compositional zoning in plagioclase in the Natong trachyandesite. Plagioclase phenocrysts in trachydacite porphyry sample F12 are notably sodic, mainly Ab_{90-99} , and occasionally show K-feldspar perthite (Or_{95}) exsolution lamellae, observed optically and also within the microprobe.

In summary, the more evolved trachyandesite and trachydacite porphyry suites contain sodic plagioclase (i.e., andesine and albite) and alkali feldspar whereas mafic basalt and phonotephrite contain Ca-rich plagioclase or labradorite.

Amphibole Mineral Chemistry

Mafic amphiboles, specifically hornblende, occur mainly as laths, tabular crystals, and four-sided diamond-shaped basal sections in the intermediate trachyandesite (OPNA5) from Natong and in the evolved phonotephrite (sample OPN8B) from Niffin. Using the Ca-amphibole classification after Leake et al. [24] and the Amp-TB spreadsheet by Ridolfi et al. [25], the amphibole composition in OPNA5 and OPN8B is calculated as magnesiohastingsite (Table 2, Figure 15), a magnesium-rich Ca-hornblende (13–14.5 wt% MgO). The composition of amphibole laths and a megacryst in OPN8B were identified as magnesiohastingsite with minor pargasite within the megacryst (Figure 15). In the same sample, hornblende is observed to be replacing early pyroxene grains which are now decomposed or resorbed [30].

Table 2. Electron microprobe analysis of amphibole in OPNA5 and OPN8B.

Sample Number	OPNA5	OPNA5	OPNA5	OPNA5	OPN8B	OPN8B	OPN8B
Point	18	19	20	21	7	8	8
Job	7	7	7	7	8	8	9
SiO ₂	40.78	40.6	40.18	40.28	38.697	40.193	39.923
TiO ₂	2.26	1.84	1.94	2.12	2.805	2.654	2.601
Al ₂ O ₃	12.36	12.96	13.41	12.79	14.028	13.382	13.984
Cr ₂ O ₃	0	0	0.01	0.01	0	0.02	0.004
FeO	12.86	11.49	12.21	12.25	11.067	10.556	11.169
MnO	0.28	0.12	0.16	0.22	0.229	0.197	0.189
MgO	13.18	14.48	13.58	13.45	13.052	13.831	13.428
CaO	12.08	12.27	12.29	12.18	12.344	12.088	12.107
Na ₂ O	2.6	2.73	2.64	2.75	2.288	2.404	2.355
K ₂ O	1.4	1.28	1.23	1.29	1.615	1.635	1.553
Total	97.8	97.77	97.65	97.34	96.125	96.971	97.339
Mineral	Zoned Hb	Zoned Hb	Zoned Hb	Zoned Hb	Hb spindle	Hb megacryst	Hb megacryst
Mode of occurrence	Phenocryst	Phenocryst	Phenocryst	Phenocryst	Phenocryst	Phenocryst	Phenocr-yst
Species	Magnesio-hastingsite	Magnesio-hastingsite	Magnesio-hastingsite	Magnesio-hastingsite	Pargasite	Pargasite	Magnesio-hastingsite

Mica Mineral Chemistry

The mica group forms distinct minerals and are not part of a solid solution series as other minerals are such as feldspars, olivine, clinopyroxene, and actinolite–tremolite. Distinct mica minerals include muscovite, siderophyllite, eastonite, phengite, phlogopite, and biotite [31]. Biotite is a common mineral phase in intermediate and felsic igneous rocks. Biotite inclusions were observed in a hornblende megacryst in OPN8B (phonotephrite) from the Niffin area. Tabular biotite microphenocrysts also occur in the groundmass of the trachydacite porphyry (F12) and are relatively Mg rich. Table 3 summarizes the EMPA results of mica in phonotephrite OPN8B and trachydacite F12. When plotted in the annite-siderophyllite–phlogopite–eastonite (ASPE) quadrilateral diagram by Speer [32] in

Figure 16, the mica in F12 classified as phlogopite (and abbreviated as “phlog” in Table 3). The mica in the evolved phonotephrite OPN8B contained more Fe and subsequently plotted on or above the 0.3 line in Figure 16 signifying it to be igneous biotite.

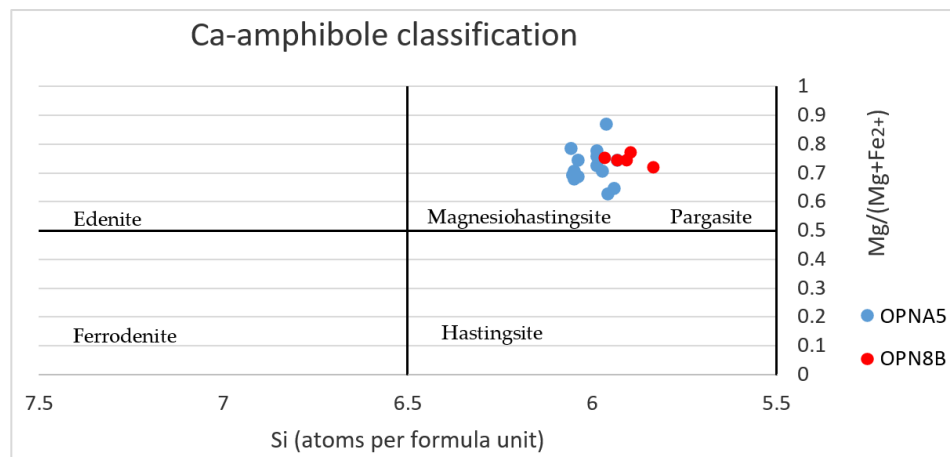


Figure 15. Amphibole chemistry for hornblende phenocrysts in the trachyandesite suite (OPNA5) from Natong and phonotephrite suite (OPN8B) from Niffin, Ambitle. Stoichiometry calculated using AMPH13.xls (Gabbrosoft.org accessed on 1 June 2022) and plotted in Excel using the Ca-amphibole classification after Leake et al. [24]. OPNA5 amphibole is magnesiohastingsite. OPN8B amphiboles comprise of both magnesiohastingsite and pargasite.

Table 3. Electron microprobe analysis of mica in phonotephrite (OPN8B) and trachydacite (F12).

Sample	OPN8B	F12	F12	F12
Point	10	1	5	7
Job	8	3	3	3
SiO ₂	35.26	38.57	38.44	40.65
TiO ₂	3.53	2.89	2.07	2.38
Al ₂ O ₃	17.47	11.41	11.26	11.46
Cr ₂ O ₃	0.07	0.03	0.05	0.07
FeO	12.35	12.86	13.49	12.72
MnO	0.19	0.15	0.18	0.21
MgO	16.08	18.03	18.02	18.98
CaO	0.06	0.00	0.02	0.01
Na ₂ O	1.47	0.82	1.14	0.71
K ₂ O	7.98	9.48	8.67	8.67
NiO	0.02	0.02	0.00	0.00
Total	94.49	94.25	93.34	95.86
Al (apfu)	2.749838089	2.022636188	2.015425253	1.974545278
Fe/(Fe + Mg)	0.3010823	0.285744138	0.295720045	0.273201555
Mineral	Biotite	Phlog	Phlog	Phlog
Mode of occurrence	Inclusion in hornblende phenocryst	Microphenocryst	Microphenocryst	Microphenocryst

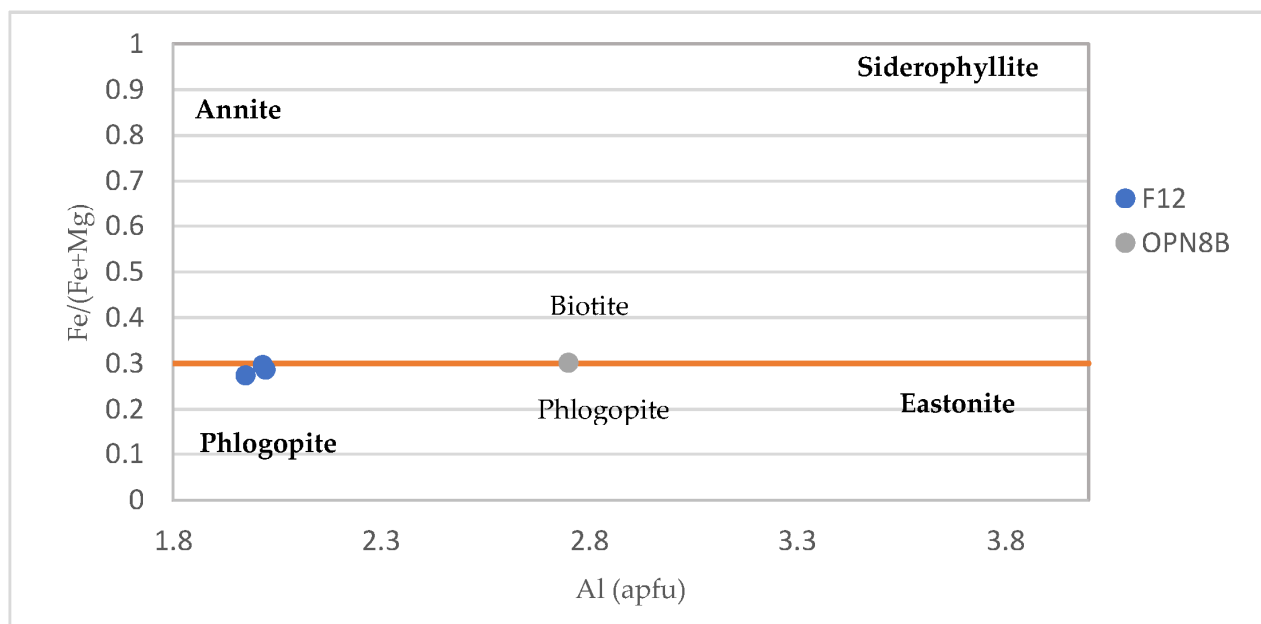


Figure 16. Biotite chemistry classified in the annite–siderophyllite–phlogopite–eastonite (ASPE) quadrilateral by Speer [32]. F12 micas are magnesium rich and therefore, may be classed as phlogopite. Biotite in OPN8B is more iron rich and can be classified as an igneous biotite.

Accessory Mineral Chemistry-Ti Magnetite, Magnetite, and Apatite

Minor and accessory minerals include magnetite or titanomagnetite and apatite. Table 4 shows these minerals observed in the mafic phonotephrite sample OPN3, trachydacite porphyry F12, and trachyandesite OPNA5. Apatite occurs in mafic, intermediate, and felsic rocks. EMPA of euhedral, trapezium-shaped apatite grains in F12 assayed 50–53 wt% CaO (Figure 9L, Table 4). Magnetite generally contained 5.7–5.8 wt% TiO₂ and ~68 wt% FeO occurring in mafic to intermediate lavas. Impurities in magnetite include Mg and Al (Table 4). Figure 9D,G,H are photomicrographs of apatite in OPNA5 closely associated with the amphibole mineral clusters. The apatite and magnetite are interpreted to be igneous in origin [33]. The apatites in the trachyandesite OPNA5 are slightly more calcic than those in F12 and OPN3. The apatite in OPN3 has more SiO₂, Al₂O₃, FeO, and MgO than the other apatite species.

Table 4. Electron microprobe analysis for accessory minerals. Titanium-bearing magnetite and apatite in phonotephrite sample OPN3. Apatite in F12 and OPNA5. All measurements in wt%.

Sample	OPN3	OPN3	OPN3	F12	F12	OPNA5	OPNA5
Litho	Phon	Phon	Phon	TD	TD	TA	TA
Point	28	29	30	8	9	24	25
Job	8	8	8	3	3	7	7
SiO ₂	0.1	0.13	2.69	0	0	0.50	0.31
TiO ₂	5.79	5.69	0.04	0	0	0	0
Al ₂ O ₃	7.83	7.32	0.37	0	0	0	0
Cr ₂ O ₃	0.04	0.03	0.02	0	0.05	0.01	0
FeO	68.44	68.04	0.85	0.12	0.1	0.40	0.16
MnO	0.81	1.07	0.08	0.08	0.09	0.08	0.07

Table 4. *Cont.*

Sample	OPN3	OPN3	OPN3	F12	F12	OPNA5	OPNA5
MgO	4.23	2.97	0.95	0.05	0.04	0.14	0.09
CaO	0.07	1.94	50.07	52.67	52.92	54.23	54.45
Na ₂ O	0	0.06	0.02	0.26	0.10	0.09	0.06
K ₂ O	0.01	0	0.04			0.01	0.01
Total	87.31	87.31	55.12	53.22	53.29	55.50	55.13
Mineral	Magnetite	Magnetite	Apatite	Apatite	Apatite	Apatite	Apatite

4.3. Whole-Rock Geochemistry

The whole-rock geochemical analysis is split into major (Table 5) and trace elements (Table 6). This is a representative summary of the geochemical data which is fully presented in the Supplementary Materials.

Table 5. Representative major element analysis of the Feni volcanic rocks.

ID	Rock ₁	SiO ₂	Al ₂ O ₃	CaO	Fe ₂ O ₃	MgO	Na ₂ O	K ₂ O	TiO ₂	P ₂ O ₅	Cr ₂ O ₃ or SO ₃	LOI	Total
F4	Ba	46.7	9.3	16.6	9.6	10.3	1.9	1.5	0.6	0.2	0.0	0.9	97.9
F5	TBa	48.3	15.3	11.5	10.6	6.4	3.5	2.4	0.9	0.5	0.0	0.4	100.0
F6	PhoT	49.1	17.8	9.0	9.8	3.8	4.7	3.7	0.8	0.6	0.0	3.0	102.6
F7	Ba	44.8	14.2	12.8	10.4	7.3	1.7	2.0	1.0	0.4	0.0	3.5	98.4
F9	PhoT	49.0	18.8	6.9	6.4	2.5	4.4	3.9	0.6	0.4	0.0	3.1	96.1
F11	Ol-Ba	47.2	10.0	15.5	10.6	10.2	2.1	1.6	0.7	0.4	0.0	1.3	99.9
F12	TD	67.0	16.0	0.5	1.5	0.9	5.6	5.8	0.2	0.1	0.0	1.8	99.3
F16	Ba	45.5	14.3	12.5	10.5	6.3	2.6	1.8	1.0	0.5	0.0	3.4	98.5
F19	Ol-Ba	44.8	13.0	14.1	9.9	8.0	1.6	1.3	1.0	0.4	0.0	1.6	95.9
F23	TBa	49.1	18.9	8.2	7.7	2.7	3.4	2.7	0.7	0.5	<0.001	2.5	96.4
OP-N3	PhoT	46.3	16.8	9.7	10.3	4.3	4.8	3.9	0.9	0.8	0.1	1.7	99.8
OP-N4C	TD	65.4	16.7	0.3	2.8	1.1	7.0	2.8	0.2	0.1	0.0	2.2	99.4
OP-N5	TA	57.7	16.9	2.0	7.7	4.0	5.0	4.0	0.5	0.4	0.0	1.8	100.2
OP-N8A	Ol-Ba	46.7	13.2	13.0	11.1	7.4	2.8	2.0	0.7	0.5	0.1	2.8	100.5
OP-N8B	PhoT	48.1	17.7	7.2	10.0	4.3	3.8	4.3	0.8	0.7	0.1	3.0	100.1
OP-NA1	TA	54.1	18.3	5.9	7.6	3.2	4.5	4.2	0.7	0.3	0.0	1.0	100.1
OP-NA5	TA	54.4	19.5	4.5	7.4	3.2	4.9	3.7	0.6	0.4	0.1	1.1	99.9
OP-BA1	TBa	49.7	18.0	9.9	9.0	4.5	3.6	1.8	0.9	0.5	0.0	2.0	100.1

¹ Ba = basalt, Tba = trachybasalt, PhoT = phonotephrite, Ol-Ba = olivine basalt, TD = trachydacite, TA = trachyandesite.

Table 6. Representative trace element, particularly rare earth element (REE), analysis of Feni volcanic rocks.

ID	La	Ce	Pr	Nd	Sm	Eu	Gd	Tb	Dy	Ho	Er	Tm	Yb	Lu	Th	U
F4	9.34	21.2	3.136	17.046	3.747	1.258	3.57	0.46	2.508	0.446	1.16	0.164	1.01	0.16	0.83	0.64
F5	15.2	34.6	5.084	25.516	5.57	1.834	5.3	0.697	3.905	0.739	1.98	0.282	1.75	0.28	1.11	0.82
F6	22.4	46.8	6.474	31.516	6.445	2.057	6.03	0.767	4.026	0.722	1.96	0.31	1.75	0.26	2.11	1.5
F7	14.4	31.2	4.444	22.916	5.034	1.769	5.02	0.706	4.165	0.791	2.11	0.337	1.93	0.32	1.35	0.85
F9	22.3	44.5	6.071	29.016	5.811	1.797	4.93	0.697	3.506	0.636	1.87	0.282	1.67	0.28	2.21	1.77
F11	12.9	29.4	4.462	23.086	5.007	1.537	4.63	0.566	2.872	0.541	1.41	0.21	1.1	0.16	0.78	0.65
F12	3.69	6.02	0.649	3.046	0.602	0.228	0.62	<0.1	0.538	<0.1	0.23	<0.1	0.21	<0.1	0.33	1.14
F14	13.4	23.2	3.566	17.586	3.291	1.221	3.86	0.513	2.985	0.576	1.62	0.228	1.38	0.23	1.2	1.03
F16	14.5	31.5	4.544	23.676	5.194	1.732	5.26	0.697	3.861	0.739	2.04	0.301	1.82	0.26	1.15	0.96
F19	10.8	24.2	3.603	18.836	4.533	1.528	4.24	0.592	3.636	0.705	1.99	0.291	1.71	0.26	0.88	0.68
F23	28	52	7.214	33.526	6.499	2.149	6.21	0.916	5.31	1.084	3.18	0.492	3.02	0.51	2.68	1.9
OP-N3	22.3	52.4	6.613	28.871	6.59	2.307	6.18	0.778	3.98	0.767	2.15	0.237	1.66	0.26	2	1.54
OP-N4C	3.38	10.9	0.857	4.463	1.152	0.523	1.03	0.194	0.854	0.168	0.44	<0.1	0.47	<0.1	0.39	0.88
OP-N5	9.59	20.5	2.762	10.893	2.754	0.871	2.37	0.364	1.959	0.336	0.97	0.156	0.86	0.16	0.91	0.92
OP-N8A	15	34.2	4.756	20.324	5.049	1.627	4.42	0.607	2.946	0.528	1.46	0.221	1.32	0.18	1.39	1.1
OP-N8B	19.4	42.2	5.292	22.86	5.828	1.817	4.79	0.616	3.369	0.671	1.87	0.246	1.71	0.22	1.99	1.4
OP-NA1	13.7	29.5	3.563	14.953	3.249	1.12	3.32	0.47	2.405	0.551	1.23	0.213	1.72	0.25	1.59	1.34
OP-NA5	20.7	41.7	4.748	19.392	4.127	1.469	3.6	0.543	2.781	0.504	1.52	0.205	1.16	0.22	2.61	1.91
OP-BA1	16.2	35.6	4.46	18.302	4.653	1.494	4.84	0.624	3.878	0.791	2.16	0.311	2.16	0.32	1.76	1.65

4.3.1. Major Elements

Major elements are presented in bivariate Harker diagrams with SiO₂ on the *x*-axis to show the main geochemical trends for the Feni magmas (Figure 17). The three main patterns observed in these plots relative to increasing silica include (1) a decreasing or compatible trend for TiO₂, Fe₂O₃, MgO, and CaO, (2) increasing or incompatible trend for Na₂O and K₂O, and (3) scattering or a mixture of incompatible and compatible behavior due to minor hydrothermal alteration and the appearance of favorable mineral phases as the melt progressively became more felsic (e.g., K₂O, Al₂O₃). The first pattern is the common fractionation trend for mafic minerals (i.e., olivine, pyroxene, magnetite) as they crystallize and subsequently deplete the melt of Fe, Mg, Ca, and Ti (Figure 17). K₂O and Na₂O positively correlate with silica but show some scatter in the more felsic rocks. The scatter in the felsic compositions most likely resulted from the variable cumulus feldspar crystals and minor alteration. Whole-rock geochemical analysis represents mineral mixtures; thus, an excess or depletion in modal mineral abundance can skew the liquid magma trends.

Al₂O₃ exhibits a steep increase from 45–50 wt% but then stabilizes and slowly decreases with increasing SiO₂. It initially behaves incompatibly in the primitive mafic melt but then behaves compatibly for rock types greater than 52% SiO₂. This is because in the basaltic melt, there is little or no mineral phase that will take up Al₂O₃ but as the melt progressively becomes intermediate and felsic in composition, minerals like amphibole, mica, and feldspar will use up the Al₂O₃.

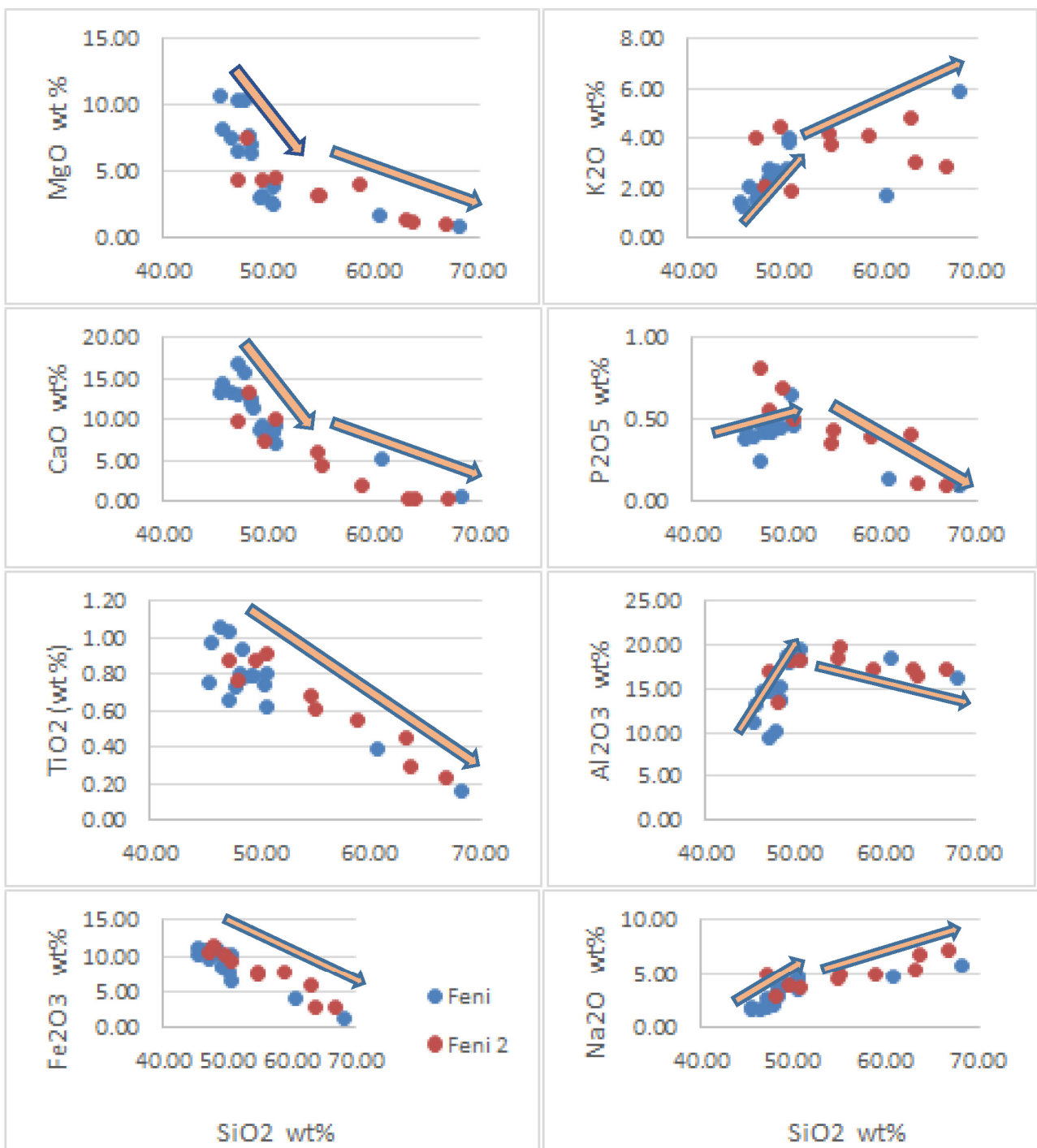


Figure 17. Major element variation plots for representative volcanic rocks from Feni Island. Blue dots are rocks collected in the first trip around Babase and Ambitle. Red dots are samples collected from outcrops in Ambitle, during the second trip. Arrows indicate major mineral fractionation trends.

An inflection point exists in most major element variation diagrams at $\sim 52\%$ SiO_2 (Figure 17). There is also a $\sim 1\%$ SiO_2 gap in the data at the point of inflection. This probably means that the rock types that form around the 52% mark (such as basaltic trachyandesite, tephriphonolite, and phonolite) were either not sampled or are absent in the Feni magma series.

4.3.2. Trace Elements

Trace elements are generally described according to their compatibility or ability to partition into a solid mineral phase or remain in the melt. Compatible trace elements are able to substitute for major elements in higher temperature mineral phases, whereas incompatible elements remain in the melt. Table 6 summarizes the REE analysis and Figure 18 presents the bivariate plots of various trace elements relative to SiO₂. Trace element trends for the Feni magmas are sympathetic to the major element trends with pronounced inflection points on many graphs (Figure 18). Relative to SiO₂, the main trace element geochemical trends in the Feni magmas include (a) a decreasing linear trend indicating compatibility and (b) a mixture of both compatible and incompatible behavior. Trace elements Sc, V, and Eu behave compatibly and decrease as SiO₂ increases (Figure 18). In contrast, the trace elements Zr, Th, Yb, Nb, and Y behave incompatibly in the mafic rocks from 45–52 wt% SiO₂ but steadily decrease in the intermediate (i.e., trachyandesite) to felsic (i.e., trachydacite) rocks (52–69 wt% SiO₂) as the magma cools. These trends are indicative of the crystal fractionation of specific mineral phases and are further elaborated on in Section 5.

4.3.3. Normalized Trace Element Patterns

Trace element concentrations are widely variable between various tectonic settings making them better geochemical discriminants than major elemental oxides. Table 6 represents a summary of the trace element analysis of the Feni volcanics, focusing on REE. These are plotted in Figures 19 and 20 in comparison to neighboring arcs within the Melanesian Arc such as Gallego in the Solomon Islands, New Britain Arc, and Manus MORB. The trace element values of all the volcanic rocks from Feni (black), Gallego (blue), New Britain (pink), and Manus MORB (red) were normalized to NMORB [34] for the spidergrams in Figure 19. The analyzed rocks of Ambitle generally have low Nb, Ti, Y, and Th (i.e., HFSE) but are enriched in Sr, Ba, Pb, Rb, K, and U (i.e., LILE). Relative to Gallego in the Solomon Arc and the New Britain (NB) Quaternary Arc, trace elements within the Feni rocks are more enriched at twice the magnitude. Trace element patterns of Gallego and the NB Arc seem to mirror the Feni rocks and are indicative of arc signatures possibly relating to the older KT arc and the current New Britain–San Cristobal Trench. In comparison to the Feni magmas, Manus MORB [27] is highly depleted in most trace elements further signifying that the Feni magmas were not generated in a MORB setting.

4.3.4. Rare Earth Elements of Feni vs. Other Arcs

REE spidergram plots were constructed for Feni, Gallego, and the Manus MORB [27] to understand REE patterns within various tectonic settings (Figure 20). Gallego on Guadalcanal represent calc-alkaline rocks within the Solomon arc to the east of the active San Cristobal Trench [1]. MORB from the Manus Spreading Centre are tholeiitic. Relative to the Solomon arc, the alkaline lavas of Feni are more enriched in REEs (Figure 20A). However, both Feni and Gallego magmas show a similar trend of enrichment in light REE (LREE), a steady decrease in middle REE (MREE), and no change in the heavy REE (HREE) forming a spoon-shape profile typical of hornblende fractionation (Figure 20). In contrast, the Manus MORB is severely depleted in LREE relative to MREE and HREE forming a dome shape (Figure 20B). This is indicative of olivine fractionation [35]. HREE in the Manus MORB is slightly more elevated than in the Feni rocks. LREE signatures in NMORB are attributed to the depleted nature of the mantle source but could also indicate olivine fractionation. The lack of a pronounced Eu anomaly in all arcs is attributed to the hydrous nature of magmas leading to the late onset of plagioclase fractionation.

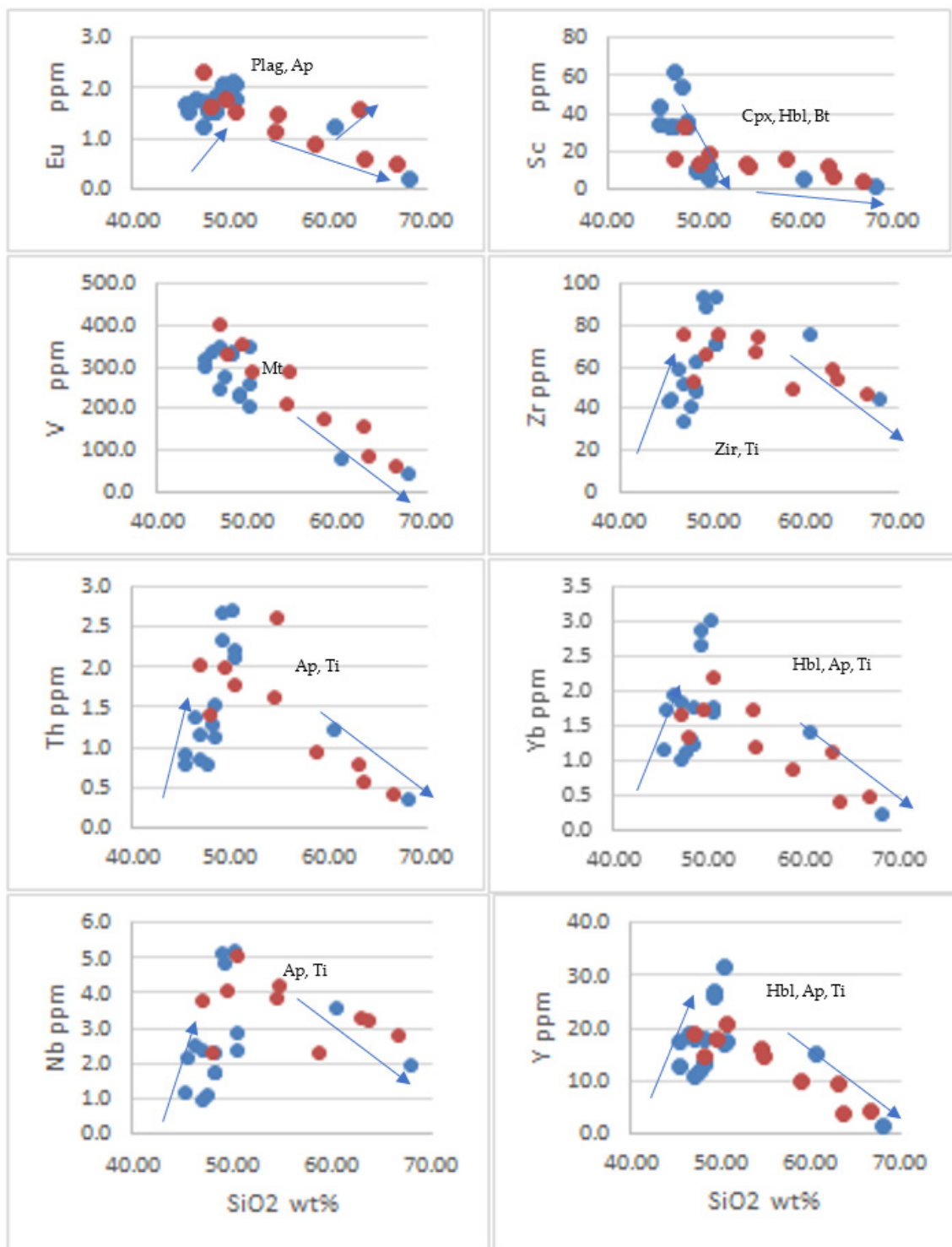


Figure 18. Trace element vs. silica bivariate plots for the representative volcanic rocks from Feni Island. The mineral fractionation likely responsible for a particular trend (as marked by the arrows) is labelled next to the plot: Plag = plagioclase, Ap = apatite, Mt = magnetite, Cpx = clinopyroxene, Hbl = hornblende, Bt = biotite, Ti = titanite. Blue dots are rocks collected in the first trip around Babase and Ambitle. Red dots are samples collected in the second trip to Ambitle.

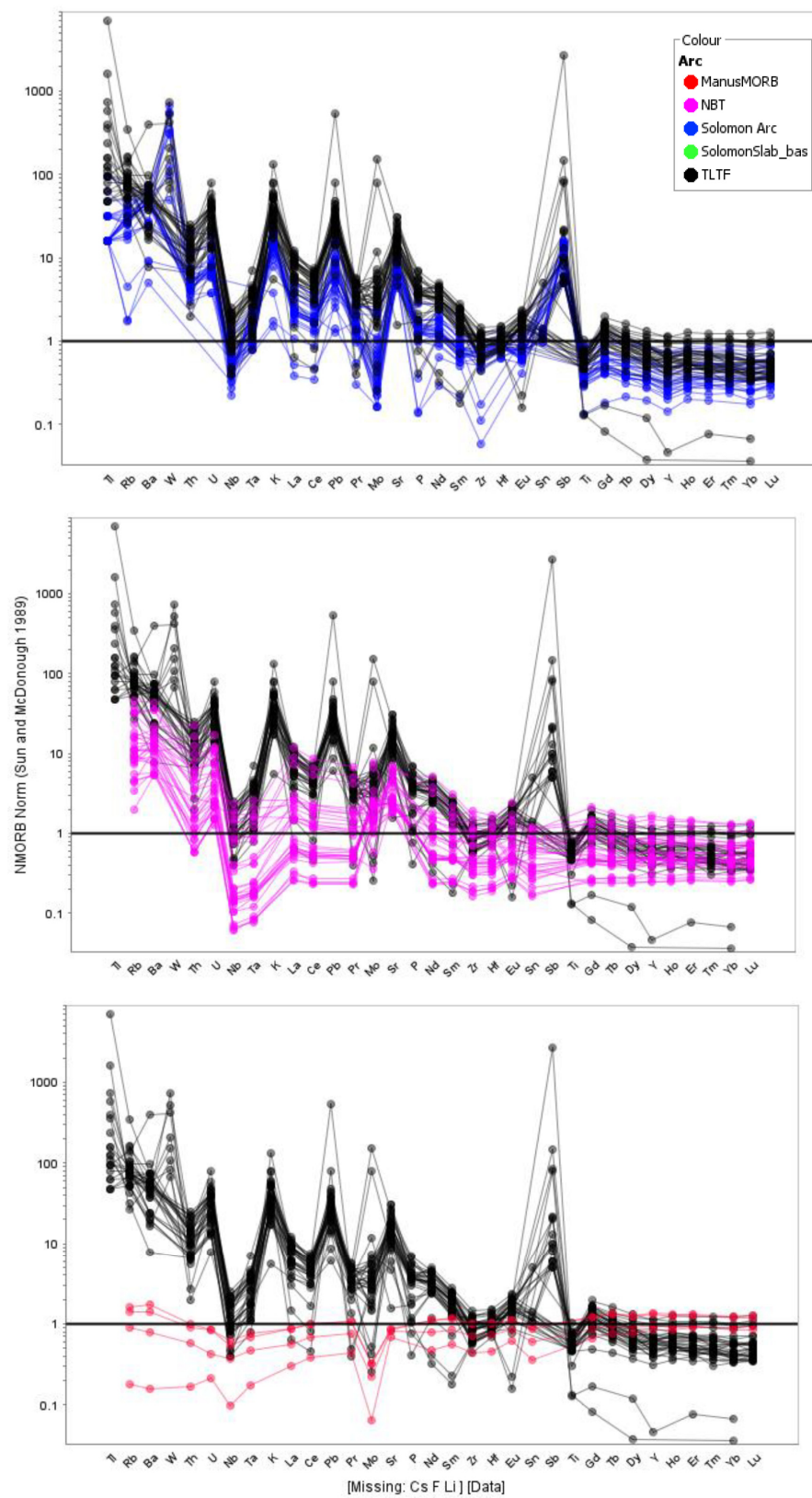


Figure 19. Spidergrams of trace element values normalized to NMORB and C1 chondrite after Sun and McDonough [34]. Black lines = Feni igneous rocks, blue lines = Gallego igneous rocks, Solomon Arc [26], pink lines = New Britain Trench Quaternary volcanics [27], and red lines = Manus MORB [27]. Plots were generated in IOGAS.

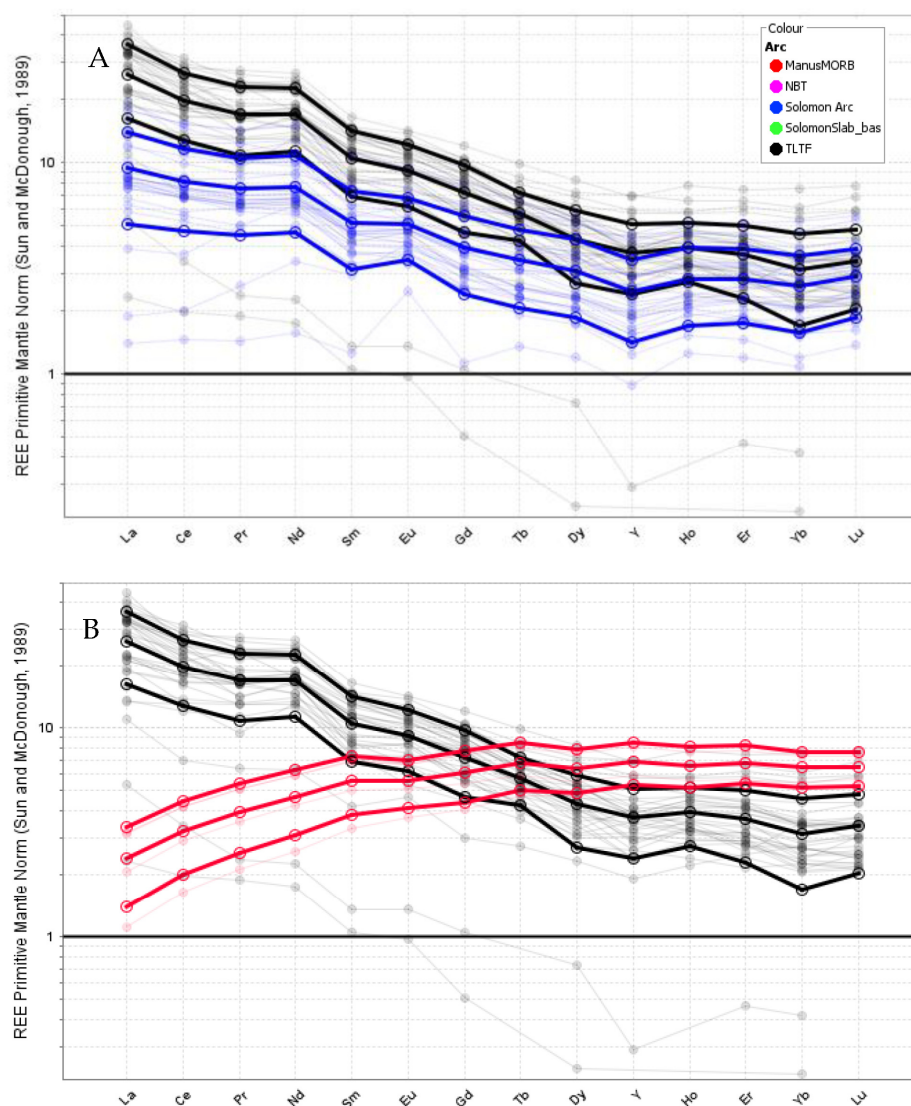


Figure 20. REE spidergram normalized to primitive mantle after Sun and McDonough [34]. Diagrams produced in IOGAS software. (A) Feni Island volcanic rocks (black) vs. Gallego igneous rocks, Guadalcanal, Solomon Islands (blue); (B) Feni (black) vs. Manus MORB (red) after Woodhead et al. [27].

4.3.5. Rare Earth Elements of Feni Volcanic Rocks

REE plots were also generated for the main lithologies from Feni. Figure 21 displays the REE patterns of the volcanic and shallow porphyry intrusions of Feni: basaltic rocks (black), phonotephrite (green), trachyandesite (grey), and trachydacite (pink). The basaltic and the phonotephritic rocks of Niffin and Balangus are most enriched in REEs followed by the intermediate trachyandesite suites of Natong (Figure 21). The felsic trachydacite porphyries are the most depleted in REEs (Figure 21).

The basalt to trachyandesite REE patterns are characterized by an enrichment in LREE, a steady decrease in MREE, and a flattening of the HREE. In contrast, the felsic trachydacite porphyry unit is distinctly depleted in REE. This was also observed by Wallace et al. [2] in their study. The overall depletion of HREE relative to LREE is characteristic of the mafic volcanic rocks of Ambitle, Lihir, and Simberi.

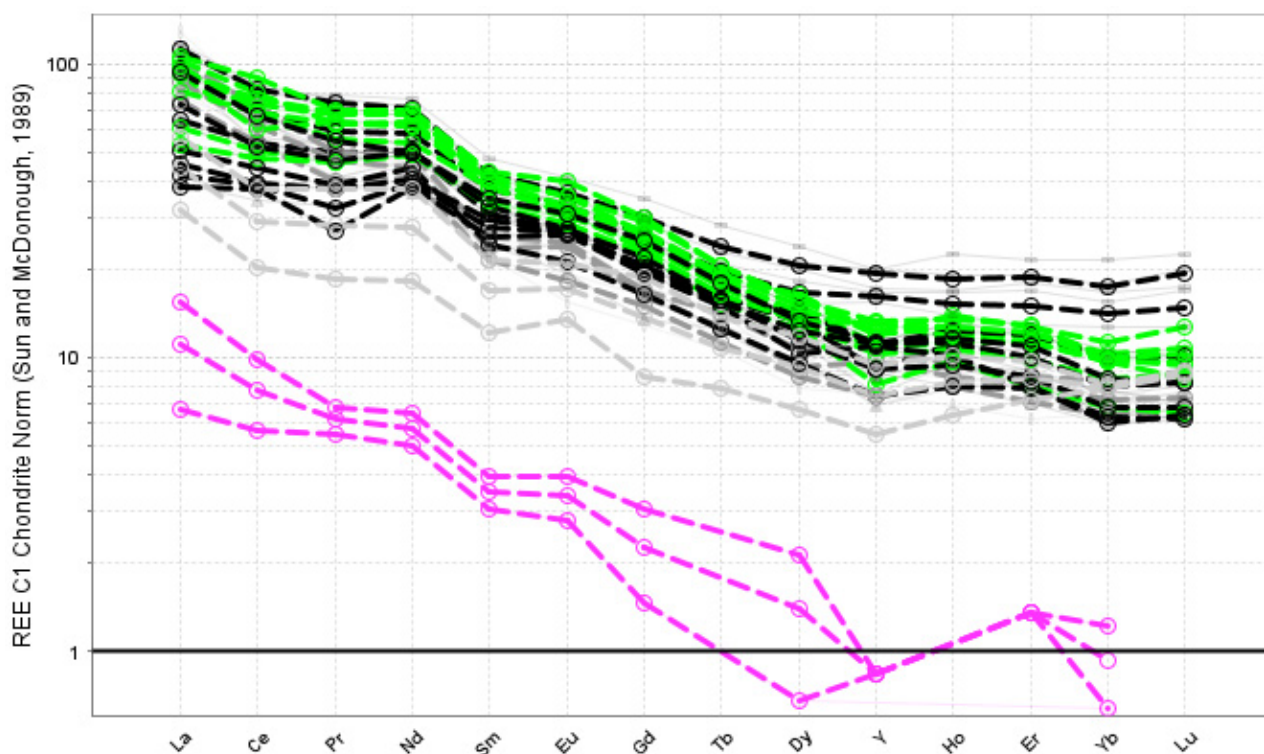


Figure 21. REE plot of all rock samples from Feni color-attributed by rock type. REE spidergrams normalized to C1 chondrite [34,36]. The black lines represent unaltered or slightly altered basalt and trachybasalt rocks; green lines represent phonotephrite from Niffin; grey lines represent trachyandesite from Natong; pink lines are felsic trachydacite porphyry (F33, F12).

Figure 22 represents REE spidergram plots for trachyandesite (A) and basaltic suites (B) in Feni. There appears to be a slight negative Ce anomaly in the Feni basaltic rocks but none in the trachyandesite. A minor positive Eu anomaly exists in the trachyandesite suite of Natong (possibly due to hydrothermal alteration or excess cumulus feldspar phases) but not in the basalt. Similarly, McInnes and Cameron [37] also showed that basalts from Simberi displayed positive Eu anomalies and negative Ce anomalies. A negative Ce anomaly is a general indication of sediment assimilation or contamination into the basaltic melt [27].

4.3.6. Discrimination and Classification Diagrams Using Trace Elements

The trace element data for Feni and the neighboring arcs were also plotted in discrimination diagrams for basalt and adakite to fingerprint their tectonic evolution or origin (Figures 23 and 24). The Th/Yb vs. Nb/Yb plot [38] in Figure 23 confirms that the igneous rocks of Feni (or TLTF), Solomon, and New Britain have volcanic arc signatures whilst the Manus MORB is normal MORB (i.e., N-MORB).

The adakite classification diagram or porphyry Cu prospectivity plots for Sr/Y vs. Y and La/Yb vs. Yb adopted from Richards and Kerrich [39] and Richards et al. [40] respectively were used to plot the Feni data relative to the neighboring arcs (Figure 24). Feni and all neighboring arcs show adakite-like signatures in the Sr/Y vs. Y plot which are attributed to the influence of garnet, clinopyroxene, amphibole, titanite, and/or zircon [39]. These minerals could occur as residual solid phases in the source that are melting (i.e., slab melt) or fractionating in a magma. However, the La/Yb vs. Yb plot did not show any adakite signatures. All arc samples generally plot in the normal andesite–dacite–rhyolite field except for one rock type from Feni which plots in the adakite field. Richards and Kerrich [39] also argued that adakite-like signatures can also result from mantle-wedge-derived magmas being influenced by crustal-level fractionation and contamination processes rather than by slab melting. Thus, adakite-like compositions are not always

indicative of slab melting, and that adakite geochemical classification schemes should be used with an open mind rather than religiously.

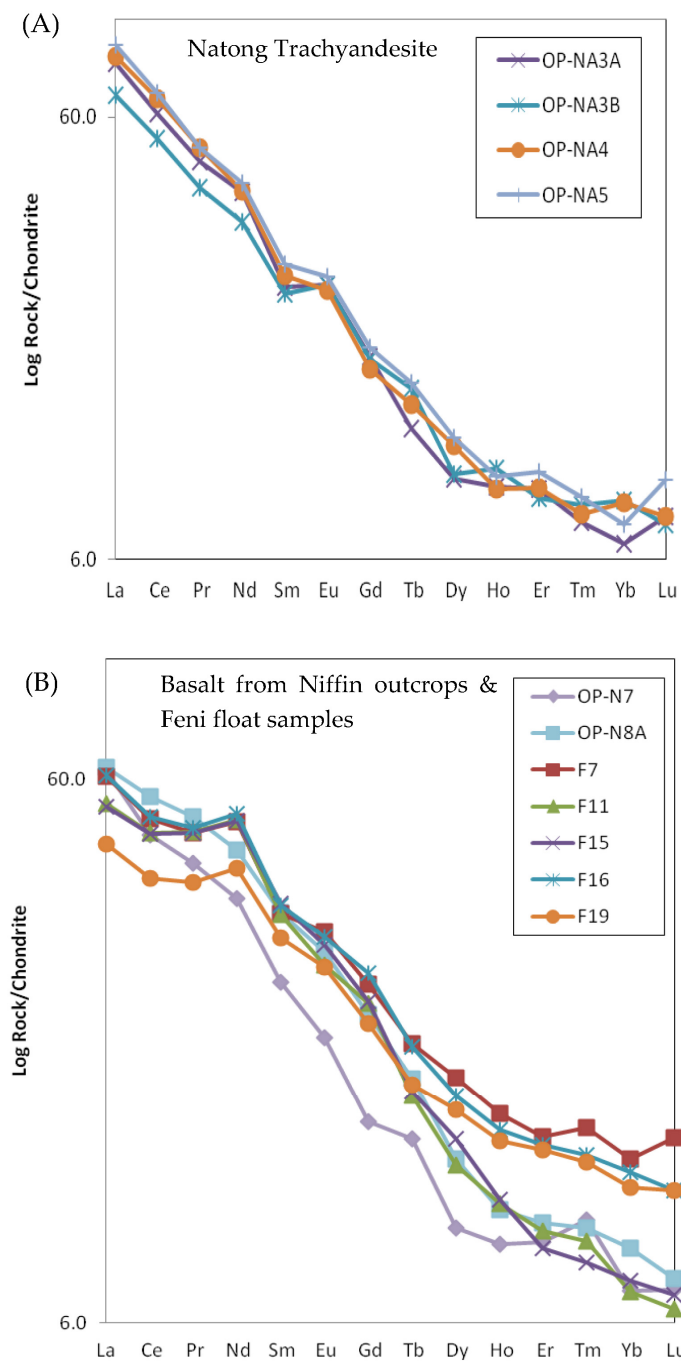


Figure 22. REE patterns of trachyandesite and basalt samples from Feni. Values normalized to CI chondrite [36]. **(A)** REE plot of the Natong trachyandesite on Ambitle. **(B)** REE patterns of basaltic samples from the Niffin outcrops and Feni in general.

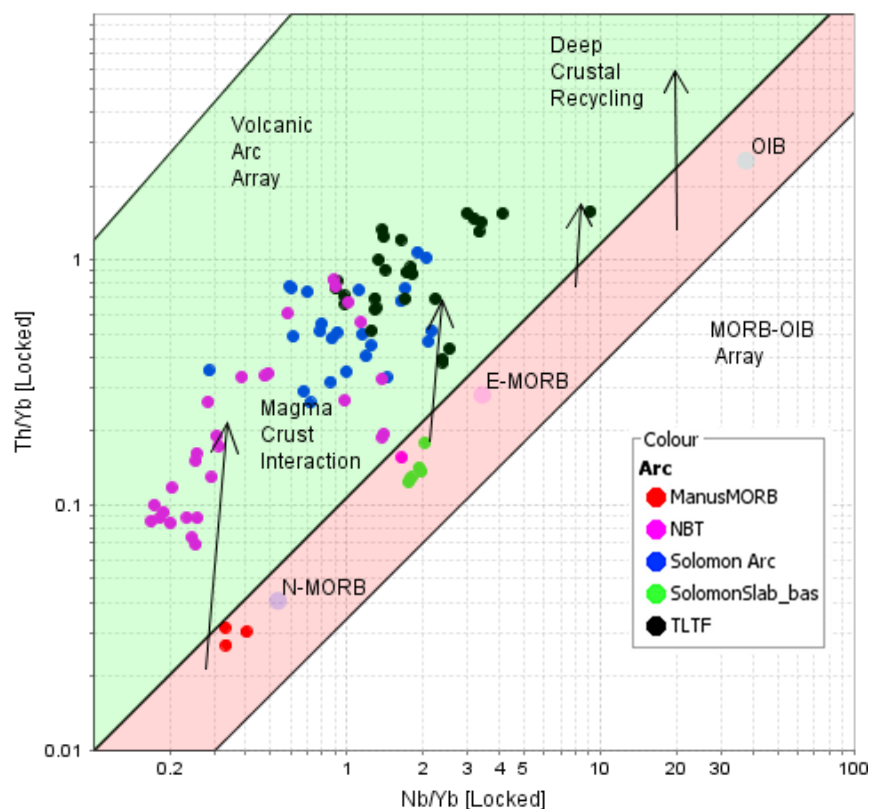


Figure 23. Th/Yb vs. Nb/Yb basalt discrimination plot after Pearce [38] for Feni (TLTF), New Britain, Solomon Slab, Manus MORB, and Gallego (Solomon Arc) volcanic rocks. Basalt classification diagram with Th-Nb as proxy for crustal input, divided into oceanic basalts, and volcanic arc basalt field. Acronyms: MORB—mid-oceanic ridge basalt, OIB—ocean-island basalt, N-MORB—normal MORB, E-MORB—plume MORB. N-MORB is depleted in trace elements compared to E-MORB.

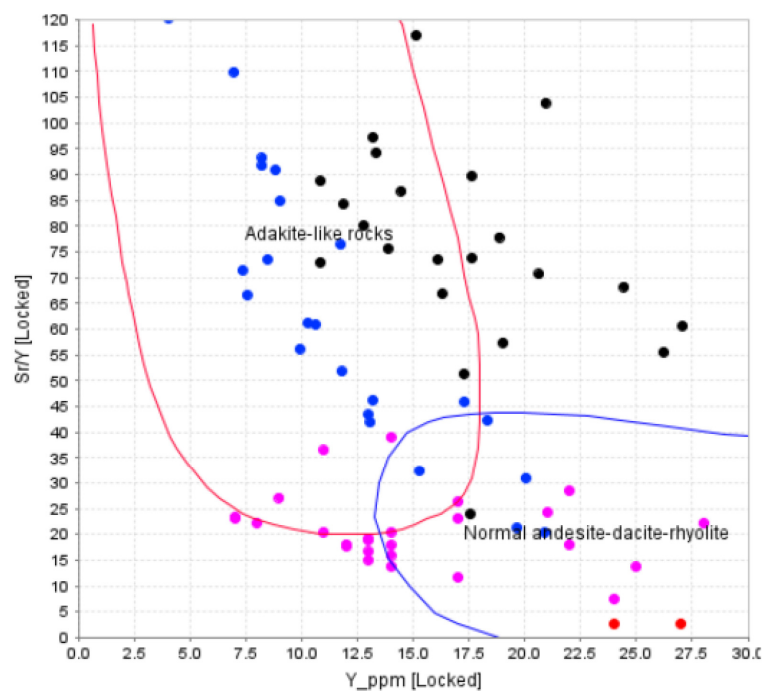


Figure 24. Cont.

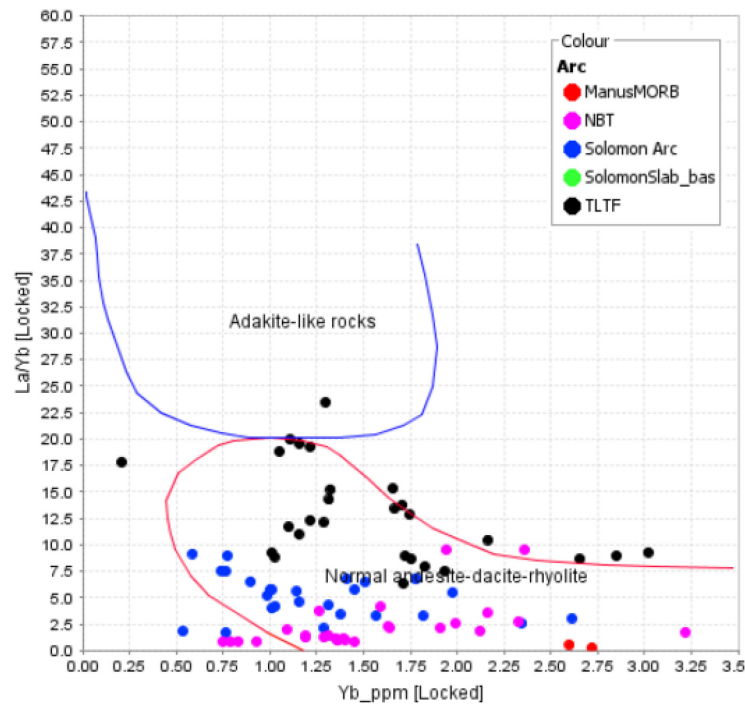


Figure 24. Adakite or porphyry Cu prospectivity plots: Sr/Y vs. Y and La/Yb vs. Yb after Richards and Kerrich [39] and Richards et al. [40]. Sr/Y vs. Y plots indicate that Feni and Solomon arc rocks are adakites whereas La/Yb vs. Yb show these are normal andesite–dacite–rhyolite (and not adakites).

Porphyry Cu-Au fertility plots were also produced in IOGAS using the Sr/MnO vs. Sr/Y diagram (Figure 25) after Ahmed et al. [41] and the V/Sc versus Sc classification diagram (Figure 26) after Halley [42].

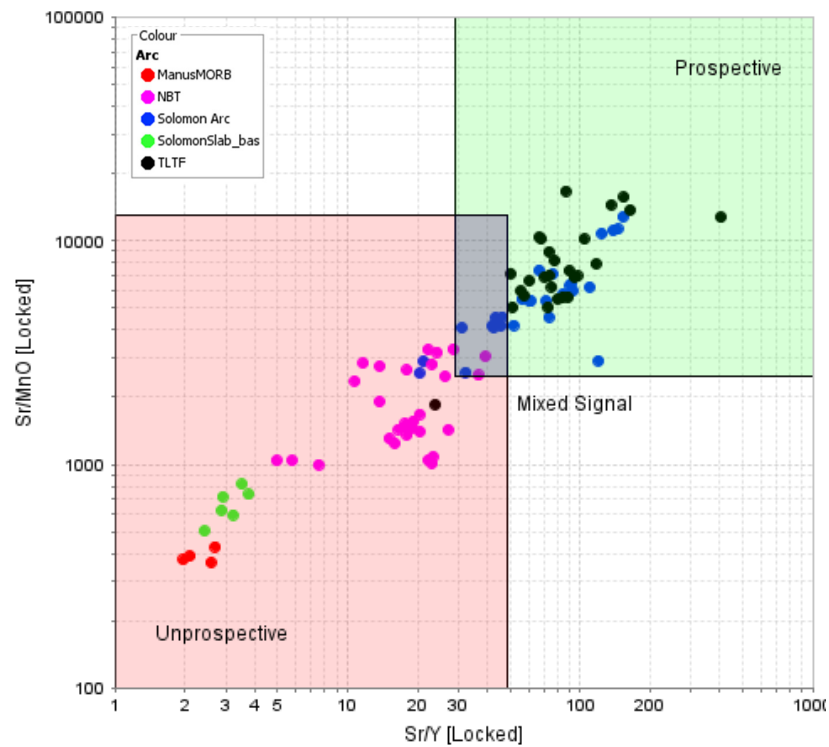


Figure 25. Porphyry prospectivity diagram Sr/MnO vs. Sr/Y [41]. Prospectivity diagram for porphyry Cu, skarn, or epithermal mineralization constructed using Sr/MnO and Sr/Y ratios. Feni and the Solomon Islands are highly prospective compared to New Britain and the Manus MORB.

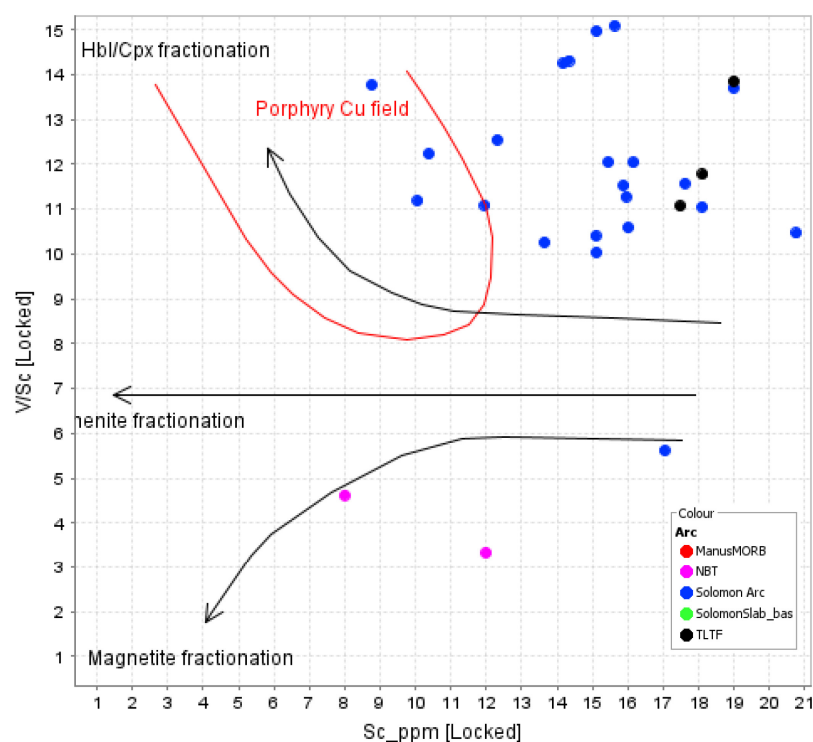


Figure 26. V/Sc vs. Sc classification diagram after Halley [42] indicative of hornblende fractionation in the Feni and Solomon arcs. Some Solomon Arc samples plot in the porphyry Cu field.

An exploration vector plot (V/Sc vs. Sc) based on Halley [42] was generated in IOGAS (Figure 26). Decreasing V/Sc with decreasing Sc signifies the fractional crystallization of magnetite, whereas increasing V/Sc with decreasing Sc signifies hornblende or clinopyroxene fractionation. Some Feni and Solomon arc rocks plot in the area of hornblende/clinopyroxene fractionation. Few Solomon Arc samples plot in the porphyry Cu field and signifies hornblende fractionation before magnetite fractionation. This is a distinctive signature for porphyry Cu-Au melts.

5. Discussion

This section aims to interpret and describe a qualitative petrogenetic model for the Ambitle volcanic and subvolcanic rocks, based on petrography, mineralogy, and trace element geochemistry. We also make comparisons to the igneous mineralogy and geochemical trends of Lihir and Simberi (Tabar) within the TLTF chain vs. the Gallego Volcanics of the Solomon Islands volcanic arc [26].

The igneous rocks of New Britain, Bougainville, and Gallego are dominantly calc-alkaline, whilst those of the Manus Spreading Centre show MORB or tholeiitic signatures (Figures 1, 4 and 23). In contrast, the TLTF volcanic islands are alkaline, K-rich, shoshonitic lavas ranging from undersaturated alkali basalts to intermediate trachyandesite and felsic trachyte or trachydacite (Figure 4). The Feni shoshonitic volcanic rocks have SiO₂ values ranging between 45% and 67% and K₂O + Na₂O values falling between 3% and 12%. In contrast, the Gallego volcanic rocks from Guadalcanal, Solomon Islands, and some NBT rocks are medium K calc-alkaline arc magmas with SiO₂ values ranging between 40% and 62% and K₂O + Na₂O values between 1 and 7%. Low K tholeiitic rocks include the Solomon slab (subducting under the New Britain trench), some New Britain arc volcanics, and Manus MORB [27].

The main volcanic rock types on Ambitle are either primitive basic magmas bearing olivine, pyroxene, plagioclase, and feldspathoid or evolved lavas with hornblende, plagioclase, feldspar, and biotite phenocrysts. The alkali basalt, mafic phonotephrite, and trachybasalt rocks are generically classified as primitive, whilst the hornblende tra-

chyandesite, hornblende phonotephrite, and trachydacite porphyry are more evolved in composition. Feldspathoids including leucite, nepheline, and hauyne are more abundant in primitive lavas and decrease with the appearance of hornblende and biotite in the evolved rock types. This pattern was also observed in the Lihir lavas by Kennedy et al. [43]. Similar rock types were also described in a petrographic and mineralogical report by Ellis [44] who analyzed six lavas from Feni and classified them as potassic phonolitic tephrite, potassic olivine nephelinite, sodic nepheline trachyandesite, and potassic tephritic phonolite. Trachydacite or quartz trachytes occur throughout the TLTF and are interpreted as late crustal melts [2].

The Feni magmatic rocks are most enriched in REE relative to the neighboring arcs of New Britain, Solomon, and Manus MORB (Figures 19 and 20). When the REE concentration of each rock type from Feni was plotted in the spidergram plots, the mafic alkaline volcanics were highly enriched in REE whilst the felsic trachydacite was strongly depleted in REE (Figures 21 and 22). This is because there is minimal or no mineral phase to absorb the REE so it remains in the mafic melt. As hornblende and apatite appear in the intermediate and felsic rocks, REE behaves compatibly starting from SiO₂ 52% as observed in Yb and Y (Figure 18).

Olivine

Olivine phenocrysts are not common in the Feni basaltic rocks but instead occur as xenocrysts. The olivine xenocryst from basalt sample OPN7 is forsteritic in composition ranging from Fo₈₇ to Fo₉₄ together with a high Ni content of 778 to 2546 ppm. Olivine analysis from basaltic and basanite samples in the Ellis [44] study are also Mg-rich or forsteritic (up to 90%) in composition. These high Mg values are comparable to mantle olivine or primary basaltic melts with Mg numbers greater than 68 and Ni \geq 250 ppm [45]. Given the abundance of other mineral phenocryst phases in the Feni volcanics, the coarse olivine crystals are interpreted as xenocrysts or xenoliths formed at greater depths and pressures. In addition, the REE spidergram plots of Feni (Figures 19 and 20) indicate hornblende and clinopyroxene fractionation in the source region but do not show signatures of olivine fractionation. We conclude that olivine fractionation occurred at greater depths or pressures in or near the mantle and that the lavas sampled in this study formed at shallower crustal magma chambers. This is supported by the Mg# vs. Ni (ppm) plot of olivine crystals in Figure 27 from two different basalt samples: olivine xenocrysts in OPN7 and olivine phenocryst in F5. F5 has low Mg and Ni content, whereas OPN7 olivine xenocryst contains higher Mg and Ni values that will have formed at greater depths and pressures within the mantle (Figure 27). Kennedy et al. [43] also interpreted that olivine fractionation in Lihir occurred at high pressure or greater depths. This resulted in erupted lavas with low Ni and MgO contents.

Clinopyroxene

The mafic alkaline volcanic rocks of Feni are rich in clinopyroxenes, accompanied by feldspathoids, Fe-Ti oxides, and minor olivine. This is very similar to the mineral composition of other mafic alkaline volcanics in other countries such as Uganda, Austria, and Italy [46–48]. Augite crystals occur in basaltic and phonotephritic rocks and typically exhibit zoning and hour-glass extinction under the microscope. The chemically zoned xenocrystic diopside crystal in phonotephrite (OPN3) shows increasing MgO and CaO composition from rim to core but decreasing values of MnO, Al₂O₃, FeO, and TiO₂ (Figure 12). The Mg-rich cores and Fe-rich rims are indicative of chemical substitution between Fe-Mg [44] and slow cooling during crystal growth possibly during ascent or residence time in magma chamber(s). Aluminium values are unusually high (Al₂O₃ up to 6.33%) and are similar to pyroxene aluminium values for Feni rocks by Ellis [44], which he attributed to being a Ca Tschermak component due to Si-Al substitutions at low pressures.

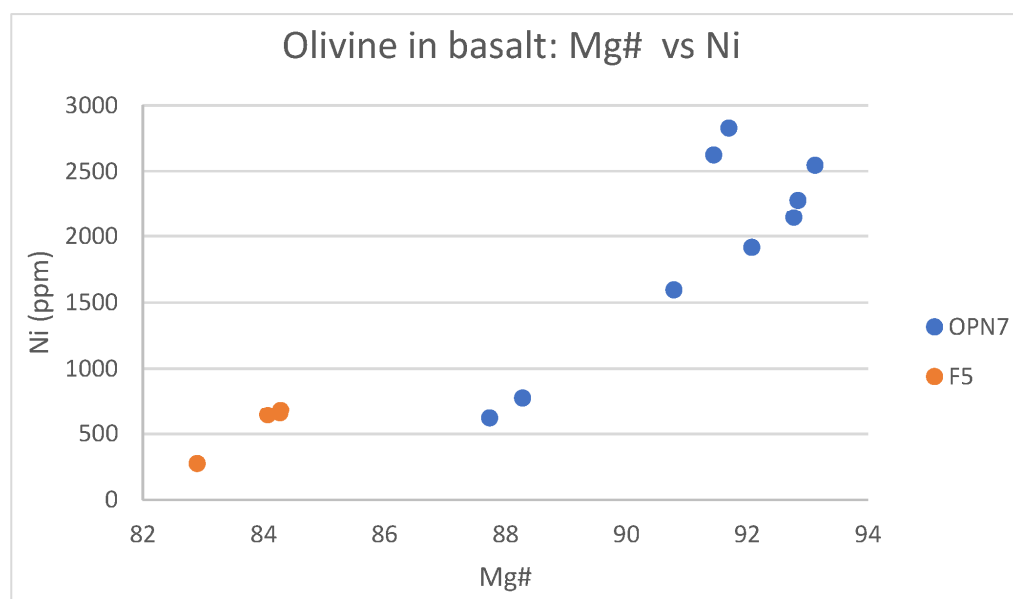


Figure 27. Mg# vs. Ni plot for olivine in basalt F5 and OPN7 indicating a high-pressure, mantle source for olivine xenocryst in OPN7 and a lower pressure or shallow depth of formation for olivine in F5.

In order to investigate the petrogenesis of clinopyroxene-rich alkaline magmas in Italy, Iacono Marziano et al. [48] conducted an experiment on basaltic melt by contaminating it with limestone (due to the abundance of carbonate-rich sedimentary country rock predating the alkaline magmas). They noted that increasing the amount of carbonate assimilation into high temperature olivine basaltic magma increased the crystallization of clinopyroxene which in turn used up most of the silica. This decreased the amount of silica in the residual melt which led to the formation of silica-undersaturated magmas such as the feldspathoid-bearing phonolite and tephrites. The presence of the negative Ce anomaly in the Feni and Simberi basalts further corroborates the hypothesis of sediment assimilation.

Similarly, McInnes and Cameron [37] described a magmatic-derived sulphate-carbonate-H₂O-alkali-rich aluminosilicate melt (SCHARM) inclusion within olivine xenocrysts from Simberi in the Tabar Group within the TLTF. They proposed that SCHARM was not in equilibrium with mantle assemblages and may have formed from the partial melting of a feldspathic phase following the initial melting of a sea water-altered basaltic slab.

Thus, we propose that both mechanisms are plausible in forming the TLTF magmas as (1) SCHARM would introduce alkali elements into the melt [37] and (2) limestone assimilation would result in the formation of clinopyroxene-rich, silica-undersaturated magmas [48]. The presence of Oligocene- to Miocene-age carbonate-rich limestone units on New Ireland, the New Ireland Basin, and the entire TLTF further corroborates the possibility of limestone or carbonate assimilation during the petrogenetic evolution of the Feni magmas [1].

Feldspathoid

Silica-undersaturated rocks bearing feldspathoids such as nepheline, leucite, and nosean are characteristic of continental rifts and intraplate hot spots. They are unusual occurrences for volcanic island arc settings such as the TLTF. McInnes and Cameron [37] proposed that volcanism in the TLTF arc is related to the extension of oceanic lithosphere overlying a subduction-modified mantle region. They also suggested that the production of silica-undersaturated arc magmas may be related to the partial melting of upwelled zones of hybrid phlogopite clinopyroxenite. Prior to upwelling, the sub-arc mantle was hybridized and enriched in CO₂ and alkali metals via a carbonate-rich slab melt or SCHARM [37]. Hauyne is also present in hornblende trachyandesite porphyry samples from Natong. It is

a feldspathoid mineral indicative of a sulfur-rich magma [49] which further supports the involvement of SCHARM as a source of sulfur, aluminium, and alkali elements.

In relation to feldspathoid fractionation in the Lihir lavas, Kennedy et al. [43] observed that fractionation at low pressure of $\sim <5$ kb produced two evolutionary trends: (1) normative nepheline in the primitive lavas due to the separation of clinopyroxene, plagioclase, and minor olivine; and (2) reduction or disappearance of normative nepheline as Ti-magnetite and hornblende formed. Our study of the Feni magmatic rocks also shows the same pattern whereby feldspathoid crystallization is suppressed as hornblende and Ti-magnetite fractionate to form the trachyandesite suite at Natong.

Hornblende

Hornblende analyses of Natong trachyandesite (OPNA5) and Niffin phonotephrite (OPN8B) from eastern Ambitle were evaluated in the Amph-TB spreadsheet by Ridolfi et al. [25] and showed the latter formed at greater depths and temperatures. Using the Amph-TB spreadsheet, melt H₂O content in trachyandesite was calculated as $4\text{--}5 \pm 0.7$ wt% with an estimated depth of crystallization at 15–19.4 km under oceanic crust and temperature ranges of 998–1025 °C [25]. In contrast, the phonotephrite sample OPN8B had a melt H₂O content of $4.1\text{--}4.9 \pm 0.7$ wt% with an estimated depth of crystallization at 19.6–24.2 km under oceanic crust at temperature ranges of 1029–1056 °C.

Hornblende composition was predominantly the Mg-rich magnesiohastingsite in the Natong trachyandesite, whereas the composition of hornblende in the Niffin phonotephrite was both magnesiohastingsite and pargasite. This signifies that the hornblende species within the two magma types crystallized under polybaric conditions or two different pressure, depth, and temperature ranges. Texturally, hornblende is observed replacing clinopyroxene in phonotephrite (OPN8B), while biotite forms inclusions within the hornblende. The hornblende-altered clinopyroxene grains are corroded or remelted. This is evidence of the recrystallization or retrograde alteration of phonotephrite caused by the introduction of a hydrous melt. Smith [50] and Cooper et al. [51] also described clinopyroxene precursors that had reactive melts percolate through them in an open system causing the crystallization or fractionation of amphibole. Thus, the prior appearance of clinopyroxene is important for the subsequent formation of amphiboles.

Plagioclase and feldspar

The more evolved subvolcanic intermediate trachyandesite and trachydacite porphyry suites contain sodic plagioclase (i.e., andesine and albite), whereas mafic basalt and phonotephrite contain the Ca-rich labradorite. However, in the hornblende–clinopyroxene-bearing phonotephrite samples F9 and OPN8B, both high temperature labradorite and lower temperature plagioclase occur together signifying a change in temperature from high to low possibly due to the influx of water or crystal fractionation.

Biotite

The biotite in the slightly hydrothermally altered trachydacite sample, F12, is the Mg-rich phlogopite, whereas the biotite in phonotephrite was slightly more Fe-rich and is thus interpreted as igneous biotite. Hydrothermal alteration and pyrite mineralization in F12 and OPNA5 signify the fertility of the hydrous Feni melts to carry metals and sulfide.

Apatite

Apatite is ubiquitous in both primitive and evolved Feni magmas but it is most abundant and strongly associated with hornblende and magnetite clusters within the hydrous trachyandesite magmas. Apatite and other phosphate minerals are the known phases that host REE. Although REE and other trace elements could not be measured in the electron microprobe, whole-rock geochemical bivariate plots of REEs vs. P₂O₅ (Figures 28 and 29) proved that the REEs positively correlated with P₂O₅. EPMA analysis of apatite crystals in Table 4 showed that the Natong trachyandesite contained Ca-rich apatite relative to the other rock types, suggesting that this may also have an influence on

the behavior of REE. Regionally, the concentrations of P₂O₅ and REEs within the K-rich, alkaline Feni magmas are higher than the tholeiitic and calc-alkaline magmas of New Britain and Gallego in the Solomon Islands. This is a common characteristic of most alkaline deposits which are abundant in phosphate minerals and REE. Thus, in addition to gold and copper, Feni and the entire TLTF also have the potential for REE exploration, research, and development under the Critical Minerals banner for green energy technology.

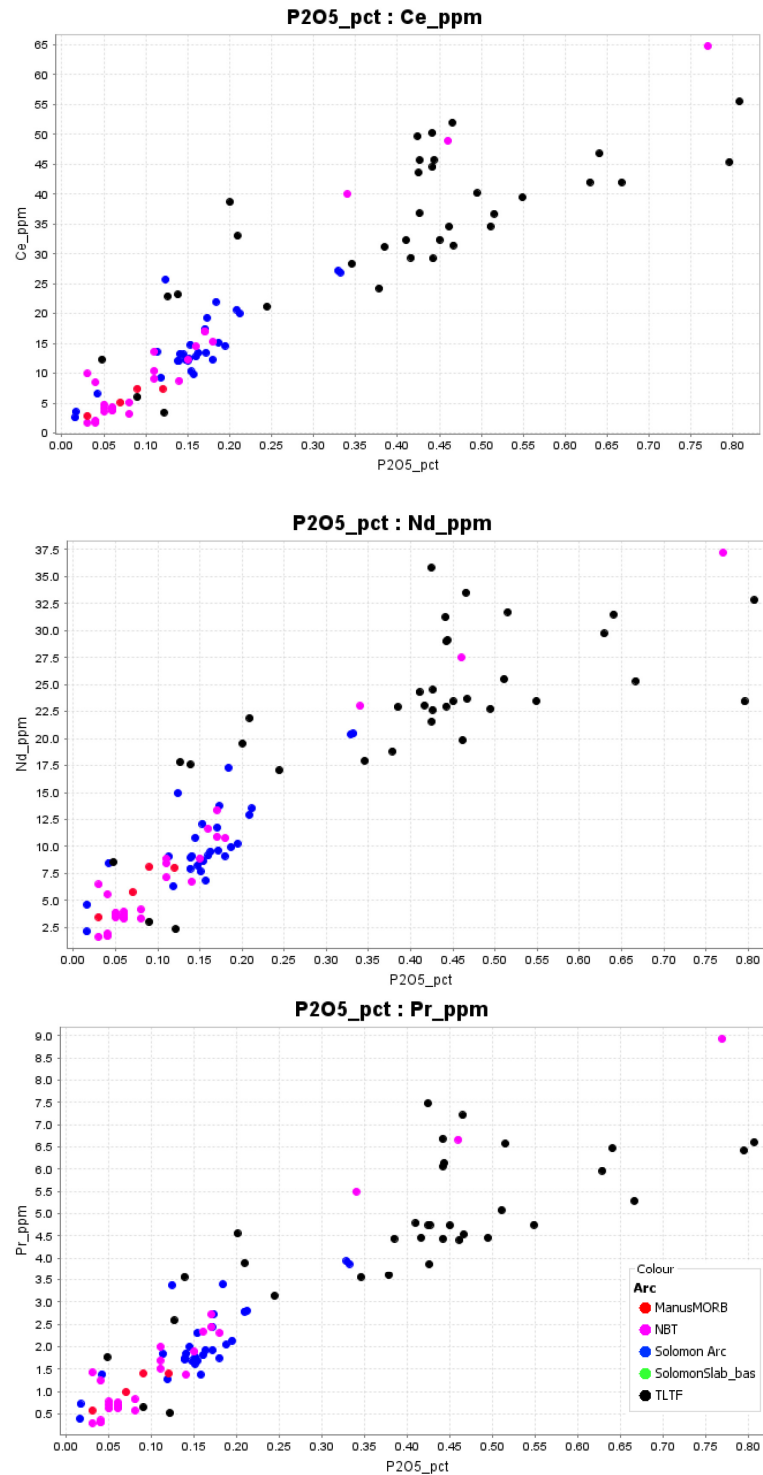


Figure 28. Bivariate plots of P₂O₅ vs. REE (Ce, Nd, Pr).

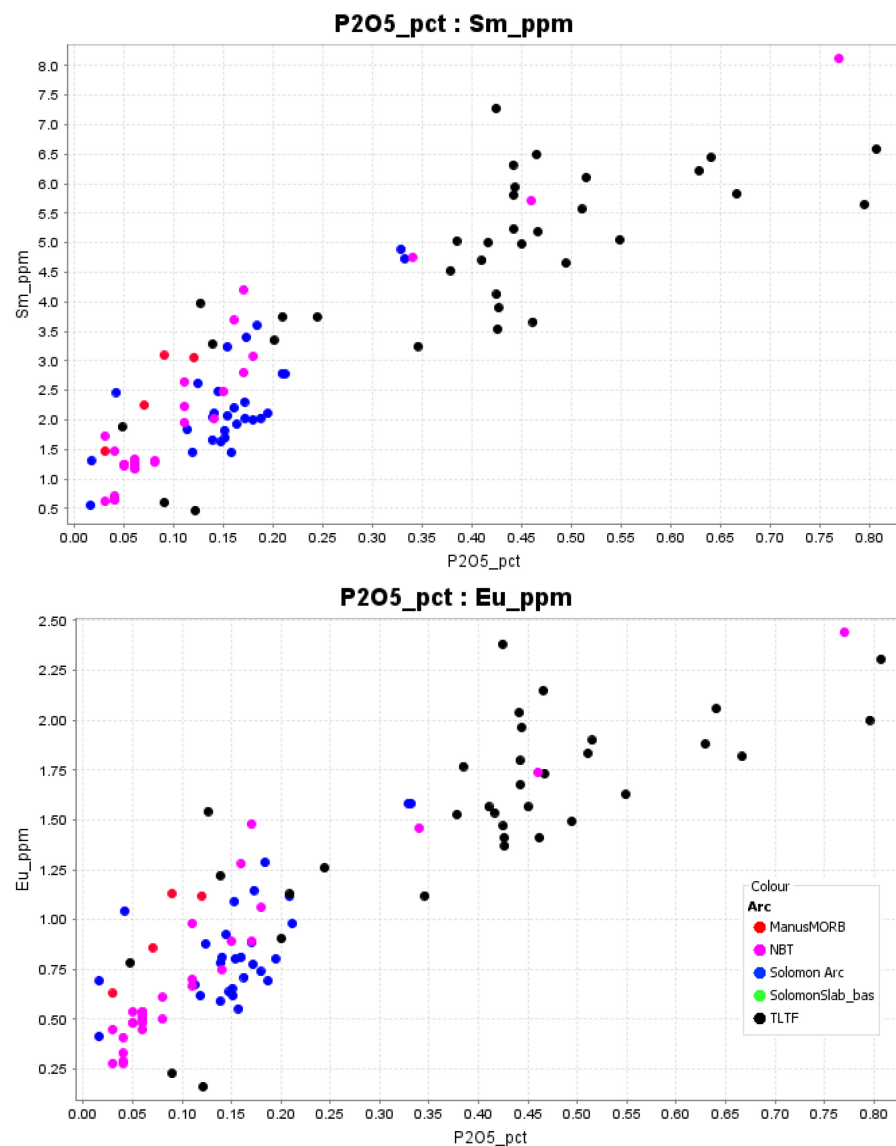


Figure 29. Bivariate plots of P₂O₅ vs. REE (Sm, Eu).

5.1. Major Element Geochemistry

The trends observed in the bivariate major elemental oxide plots are indicative of a change in fractionation of the mineral assemblages (Figure 17). At SiO₂ contents ranging from 45% (i.e., basalt) to 52% (i.e., trachybasalt and phonotephrite composition), the declining MgO, CaO, Fe₂O₃, and TiO₂ compositions indicate olivine, pyroxene, magnetite, and anorthitic plagioclase +/- amphibole crystal fractionation. In contrast, Al₂O₃, Na₂O, K₂O, and P₂O₅ behave incompatibly with silica in the mafic rocks <52%. This is because during this phase of fractionation, there is little or no mineral phase to remove K₂O and Na₂O from the primitive basaltic melt except for minor alkali feldspar and feldspathoid. As the melt fractionates and becomes more felsic, the minerals that take up K₂O and Na₂O include feldspar, plagioclase, feldspathoid, and biotite in the more intermediate and felsic igneous rocks.

From ~53% to 70% SiO₂, MgO and CaO decline gradually relative to the basic or low SiO₂ rocks. K₂O and Na₂O behave incompatibly relative to silica with the former displaying more scatter possibly as a result of variable cumulus feldspar crystals and alteration. These geochemical patterns are consistent with a change in the crystal fractionation of the controlling mineral assemblage:

- (1) Olivine, clinopyroxene, and amphibole fractionation removes MgO and Fe₂O₃ from the melt.
- (2) Clinopyroxene, amphibole, anorthite, and apatite fractionation removes CaO from the melt.
- (3) Titanite, magnetite, clinopyroxene, amphibole, and biotite fractionation removes TiO₂ and Fe₂O₃ from the melt (Figure 12, Tables 2–4)

Apatite is the main phosphate mineral that will use up P₂O₅ from the melt. It mainly occurs as a minor or accessory mineral in the mafic and felsic magmas of Feni. It is also strongly abundant in the mafic glomerocryst or cumulate phases of the Natong trachyandesite occurring alongside hornblende and magnetite. This explains the divergence or scatter in the Harker plots in Figure 17 as a result of its abundance and mode of occurrence in the various rock types.

5.2. Trace Element Geochemistry

Sc (~0–60 ppm) behaves compatibly throughout the evolution of the Feni magmas because the metal substitutes for Fe in most ferromagnesian minerals, including olivine, pyroxene, amphibole, and biotite [42]. Thus, the decreasing linear trend of Sc vs. SiO₂ is, therefore, an indication of the fractionation of these Fe-Mg silicate minerals. V is the most abundant of the trace elements in the Feni magmas assaying up to 400 ppm and also behaves similarly to Sc where it substitutes for Fe in pyroxene, amphibole, and biotite. However, V is most strongly associated with magnetite fractionation in oxidized magmas [42]. Thus, magnetite fractionation is possibly the main controlling phase for V in the Feni magmas followed by clinopyroxene, amphibole, and biotite. In addition, note that the geochemical behavior of Sc and V relative to silica is similar to TiO₂ indicating fractionation of the same minerals whereby all elements decrease with increasing silica. These elements are now compatible, meaning that at certain temperatures and compositions, certain favorable minerals will start to crystallize, incorporating these trace elements into their structure.

Zr fractionation occurs when the mineral zircon starts to crystallize in felsic to intermediate rocks around temperatures greater than 750 °C [52] and is particularly enhanced in the presence of hydrous, oxidized, and F-rich magmas [42]. Thus, the inflection point of 52% is interpreted as the composition where the magma became hydrous and hornblende crystallization began. Y and Yb are usually taken up by hornblende fractionation. Zr (30–90 ppm), Y (0–32 ppm), Yb (0–3.5 ppm), Nb (1–5 ppm), and Th (0.4–2.7 ppm) are initially incompatible and remain in the melt [53] where their concentration increases with increasing silica content from 42 to 52%. At the inflection point of 52%, all five elements decrease sharply towards 70% silica. The concentration for Eu, however, is quite low, ranging from 0 to 2 ppm. Its generally compatible trend is attributed to plagioclase and apatite fractionation which occurs throughout the Feni magma suite from the mafic to felsic composition. In general, a negative Eu anomaly is not observed in the Feni magmas and thus suggests that plagioclase did not fractionate in the source area, possibly due to the presence of water or that plagioclase crystals did not physically separate from the magma. The trachyandesite suite contains a slight positive Eu anomaly which correlates with the abundance of plagioclase phenocrysts.

Hornblende fractionation is observed in the REE spidergram plots where LREE is enriched relative to MREE and HREE forming a spoon-shaped profile (Figure 20). It is also supported by the abundance of hornblende, specifically, magnesiohastingsite phenocrysts and mineral clusters in the Natong trachyandesite. Apatite also has a strong control on REEs, U, and Th (Figures 28 and 29). In addition, Chelle-Michou [54] also discovered that titanite fractionation causes Nb, Th, U, Zr, Y, Yb, and all REEs to behave compatibly. We also observe this pattern for Nb, Th, Zr, Y, and Yb in the Feni magmas around SiO₂ 52% (Figure 18) and attribute this to the appearance of titanite along with hornblende and apatite.

6. Conclusions

The TLTF chain is a Pliocene–Holocene alkaline or shoshonitic magmatic event post-dating the older Eocene–Miocene Melanesian Arc. Its presence in the Melanesian Arc after the main cessation of subduction along the Manus–Kilinaillau Trench implies the involvement of post-subduction, extension-related magmatism related to low degrees of partial melting of a subduction-modified upper mantle. This is supported by the arc signatures of the TLTF magma geochemistry such as LILE enrichment and depletion in HFSE. High Sr/Y ratios may also suggest some involvement of slab melts either from the older Kilinaillau Trench system or from the subducting Solomon Sea Plate at the New Britain Trench immediately south of Feni.

- The main process controlling the major elemental variation in the alkaline lavas of Ambitle is fractional crystallization. High LILE (i.e., Ba, Sr, K) and depleted HFSE (Nb, Ti, Y, Th) values are typical arc signatures of the Feni rocks. The presence of LREE enrichment and depletions in MREE and HREE are signatures indicative of hornblende and clinopyroxene fractionation in the source region.
- Clinopyroxene fractionation is dominant in the mafic lavas, whereas hornblende fractionation is a major petrologic process within the phonotephrite and trachyandesite suites. Due to the presence of more feldspathoids in the primitive lavas relative to the evolved rocks, it is concluded that the addition of hornblende to the fractionating assemblage of trachyandesite (and phonotephrite) suites inhibits the crystallization of feldspathoid.
- Although plagioclase is a dominant mineral phase, REE plots lack a negative Eu anomaly, implying that there was limited or no plagioclase fractionation in the source region or that it fractionated later, potentially as a result of high-water content in the melt. Earlier higher-pressure fractionation would also inhibit plagioclase fractionation.
- The typical signatures of olivine fractionation are not observed in the REE spidergram plots of Feni. We interpret olivine as a largely xenocrystic phase with forsteritic or Mg-rich compositions and appreciable concentrations of Ni and Cr. This signifies a mantle origin for the forsterite olivine xenocrysts in the Feni basalts. Most of the mafic or basaltic rock types of Feni analyzed in this study are clinopyroxene-rich with minor olivine.
- As a result of the abundance of clinopyroxene and feldspathoids at the expense of olivine in the mafic, basaltic rocks, we are proposing the limestone assimilation model offered by Iacono Marziano et al. [48] and references therein. We believe that due to the abundance of older carbonate-rich limestone within New Ireland, NIB, and the TLTF, assimilation or incorporation during extensional periods may also contribute to the formation of localized silica undersaturated magmas. A negative Ce anomaly in basalts also supports the involvement of sediment assimilation into the melt. Magmatic SCHARM may also be responsible for contributing additional carbonate and alkali elements into the magmas [37].
- The presence of clinopyroxene is also an important precursor to the formation of amphibole as observed texturally under the optical microscope with hornblende replacing clinopyroxene. This also implies open system processes whereby fluids percolate into the magma chamber and interact with clinopyroxene crystals to form amphibole. The presence of OH-bearing mafic minerals such as amphibole and biotite, and the late fractionation of plagioclase signifies a hydrous or high-water magma content.
- Hornblende fractionation was polybaric as deduced from the compositional variation of amphibole in trachyandesite and phonotephrite. Magnesiohastingsite is the main amphibole species in both rock types but phonotephrite has pargasitic composition and formed at greater depths and higher temperatures with less melt H₂O, whereas the trachyandesite primarily contained magnesiohastingsite and was formed at shallower depths and lower temperatures with higher H₂O content. Hornblende, Ti-magnetite, and apatite are observed to occur in clusters within the trachyandesite suite.

- The abundance of apatite and the appearance of other accessory mineral phases (e.g., titanite or other phosphate minerals) in the alkaline Feni magmas past the 52 wt% SiO₂ mark also has an influence on REE and HFSE fractionation and enrichment. REE is elevated in Feni and the TLTF in contrast to the other neighboring arcs and poses an opportunity for REE mineral exploration in the TLTF (in addition to Au and Cu). Thus, apatite fractionation may also control the behavior of trace and rare earth elements in alkaline lavas.

In conclusion, the mantle source regions below Feni have been influenced by a complex history of subduction-related metasomatism, with the possible introduction of oceanic limestone and mixing of deeper and shallower mantle sources. The mechanisms most likely responsible for the petrogenetic evolution of the Feni magmas include slab melting, carbonate assimilation or contamination, crystal fractionation, and extensional tectonism leading to the upwelling or uplift of the alkaline, silica-undersaturated magmas. A schematic geodynamic model is illustrated in Figure 30.

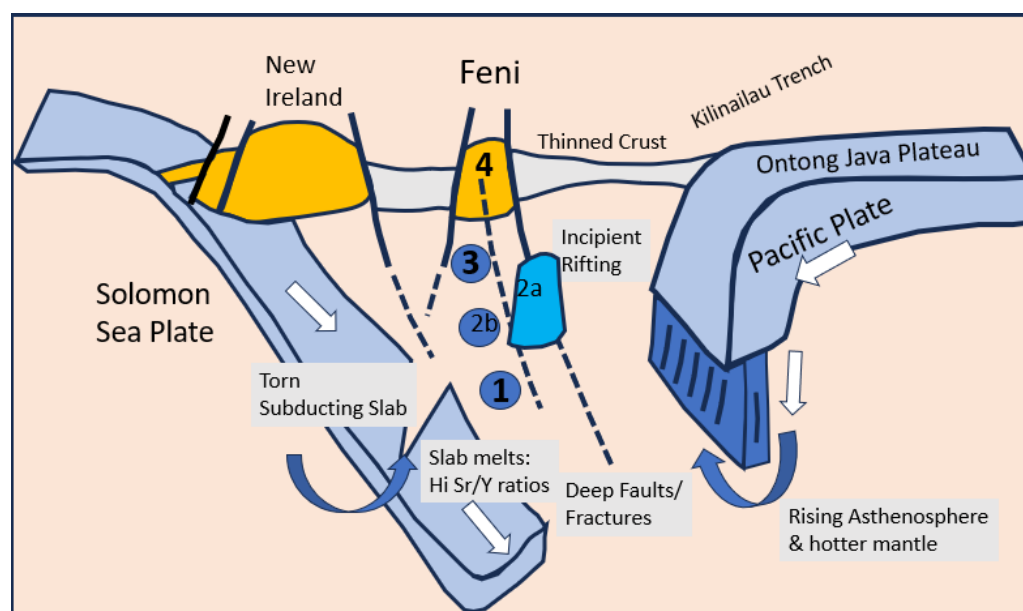


Figure 30. Geotectonic schematic model for the Feni Island Group. Feni is a horst structure within a horst and graben extended/rifted crustal-lithospheric setting. It is situated between subducting plates of opposite polarity: the subducting Solomon Sea and Pacific Plates. The mantle beneath Feni has numerous geochemical source influences including a long history of southwards subduction at the Kilinailau Trench prior to the Ontong Java Plateau impinging on the subduction zone [1]. This introduced significant quantities of ocean sediment and volatiles. The Solomon Sea Plate is subducting at a high angle and could be torn in places [55]. A hotter asthenosphere is introduced into the system as it convects beneath slab edges and/or through tears in the subducting slabs [55]. Slab melting could explain the high Sr/Y shoshonitic character of some Feni magmas. The extensional setting allows for the creation of magma pathways deep into the lithosphere and incipient local melting linked to rifting. The numbers on the diagram are related to gradually shallower zones of melting that produced the following rock types in chronological order: (1) olivine–feldspar magmas; (2a) limestone assimilation and or incorporation of SCHARM into the olivine basaltic melt which ultimately led to the crystallization of (2b) clinopyroxene–feldspathoid mafic-undersaturated magmas; (3) amphibole-dominated, hydrous magmatism, and late crystallization of albite; and (4) crustal melting that led to the crystallization of the biotite–quartz trachyte and trachydacite domes. South is situated to the left of the diagram.

Supplementary Materials: The following are available online at <https://www.mdpi.com/article/10.3390/geosciences13110339/s1>.

Author Contributions: Conceptualization, O.L.P., M.G.P. and J.O.E.; methodology, O.L.P., M.G.P. and J.O.E.; software, O.L.P.; validation, O.L.P., M.G.P. and J.O.E.; formal analysis, O.L.P., J.O.E. and M.G.P.; field investigation, J.O.E., O.L.P. and M.G.P.; writing—original draft preparation, O.L.P.; writing—review and editing, O.L.P. and M.G.P.; supervision, M.G.P. and J.O.E.; project administration, M.G.P. and J.O.E.; funding acquisition, M.G.P. and J.O.E. All authors have read and agreed to the published version of the manuscript.

Funding: This research was funded by the EU-funded Geomap project (2006–2011) under the Mining Sector Support Program (MSSP) of the Mineral Resources Authority of Papua New Guinea.

Data Availability Statement: Data presented in this research paper may be obtained with permission from the Mineral Resources Authority, email oponyalou@mra.gov.pg.

Acknowledgments: This paper benefitted from the four reviewers who took the time to review our work. We appreciate the importance of the peer review process. Fritz Bandelow, the Geomap Project (2007–2011), and the EU are acknowledged for funding this research through the Mineral Resources Authority, Papua New Guinea. This research was founded on an MOU between the University of Papua New Guinea and the University of Leicester (United Kingdom) in 2009. The good people of Babase and Ambitle islands including Paul Penua Mimfin and family are acknowledged for their hospitality and support during field excursions.

Conflicts of Interest: The authors declare no conflict of interest.

References

1. Ponyalou, O.L.; Petterson, M.G.; Espi, J.O. The Geological and Tectonic Evolution of Feni, Papua New Guinea. *Geosciences* **2023**, *13*, 257. [\[CrossRef\]](#)
2. Wallace, D.; Johnson, R.; Chappell, B.; Arculus, R.; Perfit, M.; Crick, I. *Cainozoic Volcanism of the Tabar, Lihir, Tanga and Feni Islands, Papua New Guinea: Geology, Whole-Rock Analyses and Rock-Forming Mineral Compositions*; Australian Government Publishing Service for the Bureau of Mineral Resources: Canberra, Australia, 1983. Available online: <https://nla.gov.au/nla.cat-vn1276195> (accessed on 27 September 2021).
3. Rytuba, J.J.; McKee, E.H.; Cox, D.P. Geochronology and geochemistry of the Ladolam gold deposit, Lihir Island, and gold deposits and volcanoes of Tabar and Tatau, Papua New Guinea. *US Geol. Surv. Bulletin*. **1993**, *2039*, 119–126.
4. Gleeson, K.; Butt, S.; O’Callaghan, J.; Jones, C. *Lihir Operations Aniolam Island Papua New Guinea NI 43-101 Technical Report*; Newcrest Mining Limited: Melbourne, Australia, 2020; p. 116.
5. St Barbara Limited. Ore Reserves and Mineral Resources Statements as at 30 June 2020. In *ASX Release/24 August 2020*; St Barbara Limited: Melbourne, Australia, 2020.
6. Lindley, I.D. Late Quaternary geology of Ambitle Volcano, Feni Island Group, Papua New Guinea. *Aust. J. Earth Sci.* **2015**, *62*, 529–545. [\[CrossRef\]](#)
7. Lindley, I.D. Plate flexure and volcanism: Late Cenozoic tectonics of the Tabar–Lihir–Tanga–Feni alkalic province, New Ireland Basin, Papua New Guinea. *Tectonophysics* **2016**, *677–678*, 312–323. [\[CrossRef\]](#)
8. Lindley, I.D. Matangkaka manganese deposit, Ambitle Island, Feni Island Group, Papua New Guinea: A Quaternary epithermal stratabound manganese oxide deposit. *Aust. J. Earth Sci.* **2022**, *69*, 26–46. [\[CrossRef\]](#)
9. Brandl, P.; Hannington, M.; Geersen, J.; Petersen, S.; Gennerich, H. The submarine tectono-magmatic framework of Cu-Au endowment in the Tabar-to-Feni island chain, PNG. *Ore Geol. Rev.* **2020**, *121*, 103491. [\[CrossRef\]](#)
10. O’Kane, T.P. 3-D Structure and Tectonic Evolution of the Papua New Guinea and Solomons Island Region and Its Relationship to Cu-Au Mineralisation. Unpublished B.Sc. Honours’ Thesis, Research School of Earth Sciences, Australian National University, Canberra, Australia, 2008.
11. Mackenzie, D.E.; Chappell, B.W. Shoshonitic and calc-alkaline lavas from the Highlands of Papua New Guinea. *Contrib. Mineral. Petrol.* **1972**, *35*, 50–62. [\[CrossRef\]](#)
12. Zhang, J.; Davidson, J.P.; Humphreys, M.C.S.; Macpherson, C.G.; Neill, I. Magmatic Enclaves and Andesitic Lavas from Mt. Lamington, Papua New Guinea: Implications for Recycling of Earlier-fractionated Minerals through Magma Recharge. *J. Petrol.* **2015**, *56*, 2223–2256. [\[CrossRef\]](#)
13. Holm, R.; Poke, B. Petrology and crustal inheritance of the Cloudy Bay Volcanics as derived from a fluvial conglomerate, Papuan Peninsula (Papua New Guinea): An example of geological inquiry in the absence of in-situ outcrop. *Cogent Geosci.* **2018**, *4*, 1450198. [\[CrossRef\]](#)
14. Leslie, R. *Primitive Shoshonites from Fiji: Mineralogy, Melt Inclusions and Geochemistry*; University of Tasmania: Hobart, Australia, 2004. [\[CrossRef\]](#)

15. Leslie, R.A.J.; Danyushevsky, L.V.; Crawford, A.J.; Verbeeten, A.C. Primitive shoshonites from Fiji: Geochemistry and source components. *Geochem. Geophys. Geosyst.* **2009**, *10*, 1–24. [[CrossRef](#)]
16. Cooke, D.R.; Wilson, A.J.; House, M.J.; Wolfe, R.C.; Walshe, J.L.; Lickfold, V.; Crawford, A.J. Alkalic porphyry Au—Cu and associated mineral deposits of the Ordovician to Early Silurian Macquarie Arc, New South Wales. *Aust. J. Earth Sci.* **2007**, *54*, 445–463. [[CrossRef](#)]
17. Holwell, D.A.; Fiorentini, M.; McDonald, I.; Lu, Y.; Giuliani, A.; Smith, D.J.; Keith, M.; Locmelis, M. A metasomatized lithospheric mantle control on the metallogenic signature of post-subduction magmatism. *Nat. Commun.* **2019**, *10*, 3511. [[CrossRef](#)] [[PubMed](#)]
18. Johnson, R.W.; Wallace, D.A.; Ellis, D.J. Feldspathoid-bearing potassic rocks and associated types from volcanic islands off the coast of New Ireland, Papua New Guinea: A preliminary account of geology and petrology. In *Volcanism in Australasia: A Collection of Papers in Honour of the Late G.A.M. Taylor, G.C.*; Johnson, R.W., Ed.; Elsevier: Amsterdam, The Netherlands, 1976; pp. 297–316.
19. Heming, R. Undersaturated lavas from Ambittle Island, Papua New Guinea. *Lithos* **1979**, *12*, 173–186. [[CrossRef](#)]
20. Licence, P.S.; Terrill, J.E.; Fergusson, L.J. Epithermal gold mineralization, Ambitle Island, Papua New Guinea. In Proceedings of the Pacific Rim Congress 87, Gold Coast, Australia, 26–29 August 1987; The Australasian Institute of Mining & Metallurgy: Carlton, Melbourne, 1987; pp. 273–278.
21. Carter, K.E. *P. A. 567-BABASE Annual Report to December 12, 1988*; Geological Survey of Papua New Guinea: Port Moresby, Papua New Guinea, 1988.
22. *Esso PNG Company Report, 1983*; Esso Highlands PNG Limited: Port Moresby, Papua New Guinea, 1983; unpublished.
23. Scott, E. *The Petrogenesis of Feni Islands Volcanoes, Papua New Guinea: Post Subduction Volcanic Rocks?* University of Leicester: Leicester, UK, 2011.
24. Leake, B.; Woolley, A.; Birch, W.; Grice, J.; Hawthorne, F.; Kato, A.; Kisch, H.; Vladimir, K.; Laird, J.; Mandarino, J.; et al. Nomenclature of amphiboles: Report of the subcommittee on amphiboles of the international mineralogical association, commission on new minerals and mineral names. *Can. Mineral.* **1997**, *35*, 219–246.
25. Ridolfi, F.; Renzulli, A.; Puerini, M. Stability and chemical equilibrium of amphibole in calc-alkaline magmas: An overview, new thermobarometric formulations and application to subduction-related volcanoes. *Contrib. Mineral. Petrol.* **2010**, *160*, 45–66. [[CrossRef](#)]
26. Petterson, M.G.; Haldane, M.I.; Smith, D.J.; Billy, D.; Jordan, N.J. Geochemistry and petrogenesis of the Gallego Volcanic Field, Solomon Islands, SW Pacific, and geotectonic implications. *Lithos* **2011**, *125*, 915–927. [[CrossRef](#)]
27. Woodhead, J.D.; Eggins, S.M.; Johnson, R.W. Magma Genesis in the New Britain Island Arc: Further Insights into Melting and Mass Transfer Processes. *J. Petrol.* **1998**, *39*, 1641–1668. [[CrossRef](#)]
28. Le Maitre, R.W.; Bateman, P.; Dudek, A.; Keller, J.; Lameyre, P.; Le Bas, M.J.; Sabine, P.A.; Schmid, R.; Soerensen, H.; Streckeisen, A. *A Classification of Igneous Rocks and Glossary of Terms: Recommendations of the IUGS Subcommission on the Systematics of Igneous Rocks*; Blackwell: Singapore, 1989.
29. Peccerillo, A.; Taylor, S.R. Geochemistry of Eocene calc-alkaline volcanic rocks from the Kastamonu area, Northern Turkey. *Contrib. Mineral. Petrol.* **1976**, *58*, 63–81. [[CrossRef](#)]
30. Poyalou, L.K.O. The Volcanic Rocks & Sinters of Ambitle Island, Feni Island, New Ireland Province, Papua New Guinea. Unpublished B.Sc. Honours' Thesis, University of Papua New Guinea, Port Moresby, Papua New Guinea, 2013.
31. Deer, W.A.; Howie, R.A.; Zussman, J. *An introduction to the Rock-forming Minerals*; Pearson Education Ltd.: London, UK, 2005.
32. Speer, J.A. Micas in igneous rocks. *Rev. Mineral. Geochem.* **1984**, *13*, 299–356.
33. Loader, M. Mineral Indicators of Porphyry Cu Fertility. Ph.D.'s Thesis, Imperial College London, London, UK, 2017.
34. Sun, S.S.; McDonough, W.F. Chemical and isotopic systematics of oceanic basalts: Implications for mantle composition and processes. *Geol. Soc. Lond. Spec. Publ.* **1989**, *42*, 313–345. [[CrossRef](#)]
35. Stead, C.V.; Tomlinson, E.L.; McKenna, C.A.; Kamber, B.S. Rare earth element partitioning and subsolidus exchange behaviour in olivine. *Chem. Geol.* **2017**, *475*, 1–13. [[CrossRef](#)]
36. McDonough, W.F.; Sun, S.S. The composition of the Earth. *Chem. Geol.* **1995**, *120*, 223–253. [[CrossRef](#)]
37. McInnes, B.I.A.; Cameron, E.M. Carbonated, alkaline hybridizing melts from a sub-arc environment: Mantle wedge samples from the Tabar-Lihir-Tanga-Feni arc, Papua New Guinea. *Earth Planet. Sci. Lett.* **1994**, *122*, 125–141. [[CrossRef](#)]
38. Pearce, J.A. Geochemical fingerprinting of oceanic basalts with applications to ophiolite classification and the search for Archean oceanic crust. *Lithos* **2008**, *100*, 14–48. [[CrossRef](#)]
39. Richards, J.P.; Kerrich, R. Special Paper: Adakite-Like Rocks: Their Diverse Origins and Questionable Role in Metallogenesis. *Econ. Geol.* **2007**, *102*, 537–576. [[CrossRef](#)]
40. Richards, J.P.; Spell, T.; Rameh, E.; Raziq, A.; Fletcher, T. High Sr/Y Magmas Reflect Arc Maturity, High Magmatic Water Content, and Porphyry Cu ± Mo ± Au Potential: Examples from the Tethyan Arcs of Central and Eastern Iran and Western Pakistan. *Econ. Geol.* **2012**, *107*, 295–332. [[CrossRef](#)]
41. Ahmed, A.; Crawford, A.J.; Leslie, C.; Phillips, J.; Wells, T.; Garay, A.; Hood, S.B.; Cooke, D.R. Assessing copper fertility of intrusive rocks using field portable X-ray fluorescence (pXRF) data. *Geochem. Explor. Environ. Anal.* **2019**, *20*, 81–97. [[CrossRef](#)]
42. Halley, S. Mapping Magmatic and Hydrothermal Processes from Routine Exploration Geochemical Analyses. *Econ. Geol.* **2020**, *115*, 489–503. [[CrossRef](#)]

43. Kennedy, A.K.; Grove, T.L.; Johnson, R.W. Experimental and major element constraints on the evolution of lavas from Lihir Island, Papua New Guinea. *Contrib. Mineral. Petrol.* **1990**, *104*, 722–734. [[CrossRef](#)]
44. Ellis, D.J. *A Preliminary Report on the Petrography and Mineralogy of the Feldspathoid-Bearing Potassic Lavas from the Tabar, Lihir, Tanga, and Feni Islands, off the Coast of New Ireland, PNG; 1975/29*; Department of Minerals and Energy: Canberra, Australia, 1975.
45. Gill, R. *Igneous Rocks and Processes: A Practical Guide*; Wiley-Blackwell: Hoboken, NJ, USA, 2010.
46. Tyler, R.C.; King, B.C. The pyroxenes of the alkaline igneous complexes of eastern Uganda. *Mineral. Mag. J. Mineral. Soc.* **1967**, *36*, 5–21. [[CrossRef](#)]
47. Dobosi, G.; Schultz-Güttler, R.; Kurat, G.; Kracher, A. Pyroxene chemistry and evolution of alkali basaltic rocks from Burgenland and Styria, Austria. *Mineral. Petrol.* **1991**, *43*, 275–292. [[CrossRef](#)]
48. Iacono Marziano, G.; Gaillard, F.; Pichavant, M. Limestone assimilation by basaltic magmas: An experimental re-assessment and application to Italian volcanoes. *Contrib. Mineral. Petrol.* **2008**, *155*, 719–738. [[CrossRef](#)]
49. Baldridge, W.S.; Carmichael, I.S.E.; Albee, A.L. Crystallization paths of leucite-bearing lavas: Examples from Italy. *Contrib. Mineral. Petrol.* **1981**, *76*, 321–335. [[CrossRef](#)]
50. Smith, D. Clinopyroxene precursors to amphibole sponge in arc crust. *Nat. Commun.* **2014**, *5*, 4329. [[CrossRef](#)]
51. Cooper, G.F.; Davidson, J.P.; Blundy, J.D. Plutonic xenoliths from Martinique, Lesser Antilles: Evidence for open system processes and reactive melt flow in island arc crust. *Contrib. Mineral. Petrol.* **2016**, *171*, 87. [[CrossRef](#)]
52. Watson, E.B.; Harrison, T.M. Zircon saturation revisited: Temperature and composition effects in a variety of crustal magma types. *Earth Planet. Sci. Lett.* **1983**, *64*, 295–304. [[CrossRef](#)]
53. Pearce, J.A.; Norry, M.J. Petrogenetic implications of Ti, Zr, Y, and Nb variations in volcanic rocks. *Contrib. Mineral. Petrol.* **1979**, *69*, 33–47. [[CrossRef](#)]
54. Chelle-Michou, C. *Geochronologic and Petrologic Evolution of the Magmatic Suite Associated with the Eocene Corocohuayco Deposit, and Its Role in the Genesis of the Associated Cu (-Au) Porphyry-Skarn Mineralization, Tintaya District, Peru*; University of Geneva: Geneva, Switzerland, 2013.
55. Holm, R.J.; Spandler, C.; Richards, S.W. Melanesian arc far-field response to collision of the Ontong Java Plateau: Geochronology and petrogenesis of the Simuku Igneous Complex, New Britain, Papua New Guinea. *Tectonophysics* **2013**, *603*, 189–212. [[CrossRef](#)]

Disclaimer/Publisher’s Note: The statements, opinions and data contained in all publications are solely those of the individual author(s) and contributor(s) and not of MDPI and/or the editor(s). MDPI and/or the editor(s) disclaim responsibility for any injury to people or property resulting from any ideas, methods, instructions or products referred to in the content.